RSC Advances

Study of coke deposition phenomena on SAPO_34 catalyst and its effects on light olefins selectivity during methanol to olefins reaction

Journal:	*RSC Advances*
Manuscript ID	RA-ART-06-2015-011288.R1
Article Type:	Paper
Date Submitted by the Author:	08-Sep-2015
Complete List of Authors:	Bagherian Rostami, Reza; Petroleum university of technology, Gas Engineering Department, Gas Research Center,Catalyst Research Group Ghavipour, mohammad; Petroleum University of Technology, Gas Engineering Department, Gas Research Center,Catalyst Research Group Di, Zuoxing; Tsinghua University, Department of Chemical Engineering, Beijing Key Laboratory of Green Chemical Reaction Engineering and Technology Wang, Yao; Tsinghua University, Chemical Engineering; Tsinghua University, Department of Chemical Engineering, Beijing Key Laboratory of Green Chemical Reaction Engineering and Technology Mosayyebi Behbahani, Reza; Petroleum university of technology, Gas Engineering Department, Gas Research Center,Catalyst Research Group

SCHOLARONE™
Manuscripts

Study of coke deposition phenomena on SAPO_34 catalyst and its effects on light olefins selectivity during methanol to olefins reaction

Reza Bagherian Rostami[a,*], Mohammad Ghavipour[a], Zuoxing Di[b], Yao Wang[b], Reza Mosayyebi Behbahani[a]

[a] Catalyst Research Group, Gas Research Center, Gas Engineering Department, Petroleum University of Technology, Ahwaz 63431, Iran

[b] Beijing Key Laboratory of Green Chemical Reaction Engineering and Technology, Department of Chemical Engineering, Tsinghua University, Beijing, 100084 P.R.China

Abstract

In current contribution combined measurement of products selectivity with coke deposition has been performed in order to study the deactivation of SAPO_34 during methanol conversion to light olefins emphasizing the effects of coke formation on products selectivies as well as investigation of parameters affecting coke formation. Shape selective effect of coke formation favors lighter hydrocarbon products and depending on reaction condition, 14wt% to 23wt% coke content of zeolite bed is suggested to be an appropriate range in terms of light olefins production. Comparing Hydrogen Transfer Index (defined as [alkane/(alkene+alkane)] for C_n species) as the indicator of aromatics formation with coke content of catalyst led to a meaningful relation in which coke deposition behavior can be predicted through the Hydrogen Transfer Index change during methanol to olefins reaction. Analysis of coke compounds revealed that, by increasing temperature and as the time on stream went on, relative distribution of soluble/insoluble coke shifted towards insoluble coke. Depending on the species formed at different reaction temperature, these coke species removal by air treatment varies between the temperature ranges of 550–930 K. A mathematical relation between the initial reaction condition and time on stream with average coke content is proposed as deactivation model and verified.

1 Introduction

As an alternative to the current main processes of light alkenes production (Steam cracking, Fluidized Catalytic Cracking (FCC) and Paraffins dehydrogenation), Methanol to Olefins (MTO) process by providing additional flexible root has gain more attention than ever before. Additionally, the process benefits from the availability of raw material to oil in different geographical area, the lower CO_2 emission and the lower energy consumption [1]. Among molecular sieve catalysts explored during recent decades for applying in the case of methanol conversion to light olefins[2-9] the small pore silicoalomonophosphate molecular sieve SAPO_34, with mild acid strength, hydrothermal stability and a well-defined framework with large chabazite cage and eight ring pore opening (3.8×3.8 A˚) has shown to have the best catalytic performance in the conversion of methanol to light olefins. The catalyst provide an exceptionally high carbon selectivity of about 90% to short chain olefins (C_2-C_4) at complete methanol conversion [10-13]

The catalytic processes using zeolites often include side reactions leading to the formation of carbonaceous material with catalyst deactivation as a result, defined as ‘coke’. Several studies showed that rapid deactivation of SAPO_34 catalyst during MTO reaction occur mainly due to pore blockage and mass transfer limitation associated with coke formation in its large cages and narrow pores[14, 15].

Various strategies can be taken into action in order to reduce the coke deposition and consequently increasing catalyst life time, such as optimizing the operating conditions or modifying the catalyst and decreasing the crystal size[16]. It is also important to note that, the better knowledge about the mechanism and consequently kinetics of the coke formation during MTO reaction can help us for improving this catalytic process. Fundamental works in terms of catalyst synthesis and reaction mechanism have been performed for MTO reaction [17-22].

Considerable researches have gone into MTO complex mechanism in the recent years and more than 20 different mechanisms has been proposed[23] but, due to the extremely complicated reaction route and network of MTO reaction, elucidating the reaction mechanism remains a great challenge[24]. Now there is a general consensus about the so-called “hydrocarbon pool” mechanism. Polymethylbenzenes and polymethylnaphthalenes have been proposed to be the

main hydrocarbon pool (HP) species over SAPO_34[25]. The further growth and aging of these active intermediate leads to coke formation which causes the catalyst deactivation[26]. Some observation suggested that deactivation is not necessarily initiated by polycyclic arene formation and caused by formation of bulky (gaseous) product molecules remained in the cavities of SAPO_34 and subsequently undergo sequential reactions leading to polycyclic arenes and alkanes[27]. Based on this insight, some researches have been appeared in the literature which studied the formation of coke during MTO reaction.

Alwahabi and Froment[28] related the deactivation to higher oligomerization products (C6+) which cover the acid sites or block the pores and cannot leave the catalyst. Since these species cannot be observed in reactor outlet, they used single event concept to calculate C6+ formed during reaction.

Chen et al. proposed a kinetic model for coke deposition on the basis of a mechanism in which carbenium ions as the coke precursor formed from oxygenate. These intermediates either desorb as olefins or take part in a parallel reaction to produce coke molecules[29].

Among the early works about coke deposition Voorhies's law has gained a lot of attention. This model has been derived for catalytic cracking of petroleum hydrocarbons, but extended beyond its original scope[30].

Recently, a dual-cycle model was proposed based on dual-cycle mechanism, with the assumption that only reaction between methanol and aromatic species and not alkenes leads to coke molecules formation and these species irreversibly adsorbed on one active site, thereby deactivated the site[31].

For the sake of understanding the courses of methanol conversion and catalyst deactivation and to improve the technologic and economic problems of this process, it is essential to know the behavior of coke deposition as well as its nature and its effects on catalytic performance of MTO reaction such as shape selectivity of products[15, 29, 32] in which the formation of bulky hydrocarbons via a larger-sized reaction intermediate is not allowed by the reduced free space in the cavities[33]. In this regards, the primary objective of this contribution is to provide a macro-model by measuring products selectivity with coke deposition during methanol conversion over SAPO_34. In order to achieve a better insight in deactivation by coke deposition, soluble coke

molecules and their relative distribution has been determined. As the second objective of this contribution, a simplified model is proposed as a function of initial reaction condition and time on stream for prediction of average coke content depositing on SAPO_34 catalyst bed, which is useful to reactor design when is combined with the empirical equations relating average coke content with catalyst activity.

2 Experimental

2.1 Synthesis of SAPO_34 molecular sieves

Hydrothermal synthesis of SAPO_34 was carried out using binary templates. The starting materials used in the synthesis were aluminium iso propoxide (AIP 99%, Aldrich), phosphoric acid (H3PO4 85%, Merck) and Ludox (40% aqueous solution, Aldrich) as sources of Al, P and Si respectively. Also, Tetra ethyl ammonium hydroxide (TEAOH 40%, Aldrich), morpholine (≥99%, Aldrich) were used as templates. The composition of final mixture was 1 Al_2O_3:1 P_2O_5:0.3 SiO_2: 1.5 Morpholine: 0.5 TEAOH: 60 H_2O. At first, the mixture of 20.43 gr Aluminumisopropoxide and 29 gr deionized water was stirred at 80 C for 3 h. A second mixture of 2.25 g Ludux and 9.2 g TEAOH solution was prepared and was added to first solution with stirring and mixed for 3h. Then 11.53 gr acid phosphoric and 15gr water were added dropwise to the above stirring solution. Finally the second template was added and the resulting gel was further stirred for an hour. The final 100 ml gel was aged for 24h. For crystallization, the gel was transferred into 120 ml Stainless steel Teflon-lined autoclave. The autoclave was placed at a programmable furnace. The temperature was raised to 200 C at a slope of 1C/min and maintained for 40 h. After this step, the catalyst crystals centrifuged and washed several times with distilled water to collect the product and then dried at 110°C overnight. At the end, the organic template and the water trapped within the micro pores of the as-synthesized solids were removed by calcination at 600°C for 5 h.

2.2 Catalyst characterization

Elemental analysis of catalyst was performed by Bruker S8 Tiger X-ray Fluorescence (XRF) spectrometer. The X-Ray diffraction (XRD) pattern were recorded on EQUINOX 3000 X-ray diffractometer with CuKa radiation source (k = 1.5406 Å) operating at 35 KV and 20 mA. BET surface area measurements and pore volume measurements were obtained from N_2 adsorption-

desorption isotherms at 77 K using a Micromeritics ASAP 2010 instrument. Scanning electron microscopy (SEM) was performed with a TESCAN-VEGA scanning electron microscope.

The acidity of catalyst was evaluated by temperature programmed desorption (TPD) of t-butylamine using Micromeritics AutoChem 2920 machine. Prior to TPD measurement, a sample (10 mg) was treated in a helium stream (50 ml/min) at 500 ˚C for 1 h to remove the adsorbed water. Then, the sample was cooled down to 40 ˚C and was saturated by t-butylamine at the same temperature. After saturation by t-butylamine, the temperature of sample was increased from 40 ˚C to 150 ˚C and held for 1 h so that all the physisorbed t-butylamine was removed. The temperature of the sample was then raised at a heating rate of 10 ˚C /min from 150 to 600 ˚C in the presence of helium flow.

The Thermo-gravimetric analysis (TGA), Differential Thermogravimetric (DTG) and Differential Scanning Calorimetry (DSC) measurements were performed on a TGA/DSC-1/1500 from METTLER-TOLEDO. Coked samples were heated from 30 to 900 ˚C at 10 C/min in flow of 50 mL/min of oxygen and 20mL/min nitrogen.

The quantitative composition of the soluble part of coke was obtained through GC/MS experiment in which the spent catalyst were dissolved in 20% hydrofluoric acid solution and the organic phase was extracted by dichloromethane(CH_2Cl_2), and then analyzed using an Agilent 6890/5973 GC-MS. Chlorobezene is the internal standard substance(200ug C_6H_5Cl/ml CH_2Cl_2).

2.3 Experimental reaction setup

Figure 1 shows experimental reaction system. Liquid feed with the composition of 80 weight percent methanol and 20 weight percent water pump to pre-heater to be evaporated through HPLC pump (0.01–9.99 ml/min). Nitrogen has been used as carrier gas to prevent condensation of feed and products flows in the lines. Nitrogen flow is set at constant flow of 60ml/min by a mass flow controller (0–500 ml/min). Feed diluted with carrier gas is evaporated at 250˚C in the pre-heater and then directed to the fixed bed reactor through a traced Stainless Steel tube. Catalyst was packed between quartz wool plugs inside a stainless steel (12 mm I.D. 20 cm length) tubular reactor. In the current work, 2 gr of synthesized SAPO_34 was loaded in the reactor for each run and before starting each test the catalyst bed was kept under dehydration at 733 K for about 1.5 hr by Nitrogen stream. The temperature was monitored by a thermocouple

located at the middle of catalyst bed. Products were analyzed online using gas chromatographs (Young Lin Acme 6000) with Gas-Pro and HP-PLOT-Q capillary columns with FID detection and helium as carrier gas.

A set of experiments has been performed at the temperature range of 673-733K and weight hour space velocity of (WHSV) of 1, 2 and 4 (gr MeOH.grcat^{-1}.h^{-1}). All the tests conducted in this work were operated under atmospheric pressure. In order to measure the deposited coke on SAPO_34 during MTO reaction, the tests were cut off at different time on stream (TOS) (the points in figures represent the times on streams in which the tests were cut-off) and the partial/complete deactivated catalyst was unloaded from the reactor's bed. Then the samples were sent to Beijing Key Laboratory of Green Chemical Reaction Engineering and Technology at Tsinghua University for quantitative test. Since the systematic experimental data acquired in present work was under industrial condition, the conversion was high and a distribution of coke is expected as it is inherent to a fixed catalyst bed even at lower conversion, although the uploaded coked samples represented an acceptable uniform deposition of coke species with no perceptible color difference. Thus it is reasonable that the coke data is the average coke content deposited along the reactor bed. By deployment of the obtained experimental data in building a model, information of MeOH conversion data can be avoided along the catalyst bed which results in the model to be applicable for prediction of catalyst coke content under initial condition.

3 Results and discussion

3.1 Catalyst characterization analysis

The X-Ray diffraction patterns of the samples prepared by mixed-template methods (Figure 2) confirmed the SAPO_34 structure type (CHA structure). The intensity and peak position of each peak match well with that of reported for SAPO_34 material [34]. On the other hand, there is no additional peak of impurity phase in the samples patterns. Practically no loss in crystallinity was observed when the synthesized catalyst was heated at 600 ˚C in order to remove organic template and the water trapped within the micro pores of the synthesized SAPO_34, confirming their thermal stability under calcination conditions.

Scanning electron microscopy (SEM) photographs of the synthesized SAPO_34 catalysts are presented in Figure 3. As it is illustrated in the micrographs, the typical cubic-like rhombohedra morphology can be clearly observed the synthesized SAPO_34. The size of randomly selected particles are also shown in Figure 3. The average particle size of the synthesized SAPO_34 was1.6 μm. Generally large crystal size leads to diffusion limitation in which the reactions are controlled by limitation of both methanol (MeOH) and dimethyl ether (DME). On too small crystal size a relatively large quantity of MeOH and DME scape the SAPO_34 pores before being transformed, hence resulting in lower olefins selectivity. Physicochemical properties (X-ray fluorescence (XRF), Brunauer–Emmett–Teller **(**BET) and Temperature Programmed Desorption (TPD)) of synthesized SAPO_34 catalysts are listed in Table 1. The X-ray fluorescence (XRF) results show the amount of phosphorous has been decreased from 49.82 in starting gel to 43.65 Wt% in final catalyst which apparently confirm the phosphorous replacement by silicon and hydrogen to produce bridging hydroxyl group (-SiOHAl-) as Brønsted acidic sites in the neutral framework of alumino phosphate ($AlPO_4$) molecular sieve[35]. In the present work acid strength distribution and total acidity were measured by Temperature Programmed Desorption (TPD) of t-butylamine. The t-butylamine is a suitable base for TPD test. Due to its molecular structure and its high vapor pressure t-butylamine do not have diffusional limitations in the microporous zeolite, hence giving a more

accurate result than the adsorption of ammonia. It has been well noted that strength of the acid sites can be related to the temperature in which alkyamines or ammonia are desorbed from acidic centers[36, 37].

Generally, low temperature desorption peaks at 150-300˚C are assigned to the weak acid sites. Desorption temperatures of 300-450˚C and 450-600˚C are also attributed to the moderate and strong acidic sites respectively which are generated by the incorporation of silicon atoms into the framework of SAPO-34 molecular sieve by different mechanisms[38]. It has been well-stablished that strong acid sites have significant effects on coke formation reaction such as cyclization and hydrogen transfer reaction and preferentially these sites are deactivated by coke molecules [39]. The higher density of strong acid sites leads to the faster catalyst deactivation. In fact optimization of acid strength distribution to mild and moderate have been proven to have a positive role toward light alkenes selectivity, low coking rate and longer life time. The synthesized SAPO_34 with two moderate weak and medium acid sites and a low content of a strong acid site showed more than 90% selectivity to olefins at near complete methanol conversion and proper life time.

3.2 Effect of coke deposition on product selectivity

The evolution of MTO products selectivities and conversion with the coke content at different industrial operating conditions (different temperature and contact time) is shown in Figure 4 to Figure 6. When calculating conversion levels, dimethyl ether has been counted as a reactant instead of a product[40, 41], as equilibration between methanol and dimethyl ether (and water) is assumed to occur before production of hydrocarbons. As it can be seen, coke deposition in MTO reaction influences products selectivities significantly, particularly at higher coke content. The results clearly show that the ethylene and methane mole ratio increase in the whole time during reaction as coking proceeds. The results show higher temperature favor methane formation. Generally methane was suggested to be a primary product formed directly from methanol [42-44] or a product of the large molecules such as coke. Both mechanisms may take part in the methane formation. According to the second mechanism, the high selectivity of methane at high coke contents comes from the reaction between the surface methoxy group and coke molecules[39]. Increasing methane selectivity versus coke content is owing to the deactivation of hydrocarbon pool species which are responsible for the MTO reaction products.

Propylene selectivity increased with a slight trend as coking proceed during MTO reaction. slight increasing of propylene selectivity with coke content followed by a sudden decrease which resulted from catalyst deactivation. It is also shown that higher and lower temperatures favors ethylene and propylene formation respectively (Figure 7). It is also observed that butene has a decreasing trend versus coke content. One reason for the increase in ethylene selectivity is therefore from the decreases in selectivities to propylene and butenes. Propylene and butenes are more reactive than ethylene. They can undergo oligomerization more easily to form bigger oligomers that would be trapped in the cages of SAPO_34. As temperature increases, these oligomers crack to form ethylene.

These trends could be explained by considering two reasons. Firstly, the effect of coke shape selectivity, favoring the formation of smaller molecules when the void volume in the cavities is reduced by coke and the second reason is that, product diffusion out of the catalyst crystals is hindered by the coke molecules, thereby favoring ethylene diffusion.

Under MTO conditions studied in this work, the SAPO_34 showed 85% selectivity to light olefins ($C_2^=$, $C_3^=$) and about 92% selectivity to olefins ($C_2^=$, $C_3^=$, $C_4^=$)(The UOP/Hydro MTO process provides up to 80% yield of ethylene and propylene at near complete methanol conversion [10]). The results in Figure 8 demonstrates the variation of 1.05 to 3 for $C_2^=$ to $C_3^=$ mole ratio showing the flexibility of MTO process to help meet the growing demand for ethylene or propylene. According to the results obtained here, 14Wt% to 23Wt% is an appropriate coke content range in terms of acceptable olefins production in MTO process.

DME breakthrough appears after 23 wt% coke content (Figure 9), reflecting the signal of severe SAPO_34 deactivation and suggests that the catalyst surface has been essentially covered by coke. From a mechanistic view, Methanol to DME reaction during MTO reaction is assumed to be initiate at very weak acid site and these weak acid site are active after deactivation of SAPO_34 catalyst because coking reaction occurred on strong acid site[45].

Figure 10 illustrates HTI defined as the [alkane/ (alkane + alkene)] for C_2 and C_3 hydrocarbons. As it shown, increasing WHSV (decreasing contact time) resulted in lower HTI corresponding to lower selectivity of ethane and propane as the secondary products of MTO formed via hydride transferring reaction. HTI as the indicator of aromatics formation[46, 47] was

plotted with coke content of SAPO_34 versus TOS (Figure 11). As it can be seen, coke species followed a two-step deposition, fast deposition (high HTI), happened at lower time on stream showing high aromatization reaction which results in faster coke formation and slight deposition (low HTI). It is obvious that these two step was followed by HTI figure in which HTI rate decreases with a slight reduction in its value as coke deposition rate declines with a slow increase in carbon deposits content of catalyst. As a matter of fact, heavier poly cyclic aromatic are formed with further transformation of hydrocarbon pool (HP) intermediates (MBz) which is governed by aromatisation reactions. According to the observed meaningful relation, we may reach the conclusion that the rate of HTI change can be an important indicator for coke deposition behavior on SAPO_34 during MTO reaction.

3.3 Coke analysis

3.3.1 Effect of initial reaction conditions on coke formation

3.3.1.1 Effect of space velocity

Coke deposited on the catalyst was determined by thermogravimetry. Figure 12 demonstrates the evolution of carbonaceous material deposition. As it shown coke formation follows a sharp trend at lower time on stream. After reaching to a specific coke content, coke formation rate decrease with slow increase carbon material content of catalyst till complete deactivation. This is due to the shape selectivity which affect the coke formation reactions. It is also clear that increasing space velocity leading to faster coke deposition. Recent experimental and theorical works on HP mechanism has firmly shown that MTO mechanism governed by cyclic organic reaction center (methylbenzenes (MBz)) [48]. A few amount of these organic species formed during induction period and grow by increase in olefins yield. MeOH and DME as the methylation agents react on these reaction center for the assembly of light olefins. Due to their dimension these organic species are trapped by SAPO_34 topology. Increasing methanol feed to the catalyst bed results in the more contribution of methanol reaction on MBz, Hence more light olefins will be splited-off which participate in a growth in MBz species quantity. Besides, further aging of MBz species forms polycyclic aromatics which significantly reduce reactant accessibility to the catalyst sites by mass transfer limitation. Chen et al. [29], Benito et

al. [49] showed that the coke deposition is influenced by the reaction conditions including space velocity, methanol partial pressure and temperature in MTO reaction over SAPO_34. Faster coke deposition by WHSV was proved in Hao Hu et al. work[50]. However, Guozhen Qi et al.[51] showed that coke deposition during the MTO reaction over SAPO_34 at constant temperature essentially depends on the cumulative amount of methanol fed to the catalysts. It is important to be mentioned that cumulative amount of methanol become to be important at nearly complete conversion of methanol. Because low conversion results in the unreacted methanol to exit from outlet of reactor.

3.3.1.2 Effect of temperature

The effect of temperature on coking formation rate has been found to be complex in literature. Chen et al.[29] And Qi et al.[51] suggested as reaction temperature rises, coke formation rate become faster, while Marchi and froment[52] showed that lower temperature favors coking. Xianchun Wu et al.[53] reported that higher temperatures lead to faster catalyst deactivation due to coke formation, while lower temperatures lead to faster catalyst deactivation due to oligomer blockage of SAPO_34 pores. Yingxu Wei et al. [54] reported , a new kind of non-aromatic hydrocarbon (diamondoid hydrocarbons) causes catalyst deactivation at reaction temperature of 300–325 °C. This complex behavior can be related to the fact that chemical steps of coke molecules as well as their retention within the pores or on the outer surface of the catalyst, while both the types of chemical steps and the cause of trapping depend on temperature. [55] Figure 13 and Figure 14 demonstrates the effect of temperature on coke formation during MTO reaction. It was found that higher temperature increases coke deposition and results in faster deactivation. Besides, coked samples at different reaction temperature produced seemingly different color coming from the innate structures of coke species. This suggests that changing temperature changes the formation rates of coke with different structure. As a result, rising temperature accelerates heavier coke molecules formation by increasing their own reaction rates. In summary, at low temperature, formation of oligomers and diamonoid hydrocarbons are responsible for catalyst deactivation, but rising temperature results in the cracking of these species. On the other hand, with increasing temperature, larger poly-cyclic aromatic are formed and graphitic materials deposition rate increases. This increase by temperature in weight percent

of heavy coke considered as insoluble coke deposited on the catalyst is demonstrated in Figure 17.

In order to find a better understanding of a SAPO_34 crystal deactivation of by coke, a schematic 2-D cross-sectional view of a deactivated SAPO_34 cubic particle is simulated in Figure 15. Confocal fluorescence measurements confirmed a fast formation of methyl-substituted aromatic compounds at the corners and edges of the SAPO_34 catalyst crystal and the majority of these species remains located at the edges of the crystal (Figure 16)[56]. Further aging of these species leads to larger coke species formation which prevents the reaction front to move towards the center of the crystal through blockage of the access of the reactant to the inner cages first by coke molecules (or coke precursors) formed in the cages near the outer surface then by coke molecules deposited on the outer surface leading to fast catalyst deactivation.

Thermo-gravimetric analysis (TGA), Differential Thermogravimetric (DTG) and Differential Scanning Calorimetry (DSC) profiles of SAPO_34 catalyst deactivated samples at different reaction temperatures and a WHSV of 2 (g of methanol) (h. g of catalyst) $^{-1}$ are shown in Figure 18 and Figure 19. Apparently, the deactivated SAPO-34 catalysts first go through a dehydration stage in a temperature range of 333–443 K. The peaks located at this range attribute to the evaporation of physically bound water. A distinctive weight loss was observed in a temperature range of 550–930 K. This weight loss was accompanied by an exothermic peak corresponding to the coke decomposition stage. Coke decomposition start at 550 K and 700 K for reaction temperature of 673 K and 733 K respectively, indicating different types of coke have been formed at different reaction temperatures which confirm increasing insoluble coke contribution in coke content shown in Figure 17.

Figure 20 shows the percentage of soluble and insoluble coke as a function of the percentage of coke formed at 703 K on SAPO_34. According to the figure wt % percent of soluble coke passes through a maximum by increasing coke content. It is also clear that insoluble coke in not formed at low coke content and appears at higher coke content. This behavior, which can be observed with most zeolites, shows a consecutive mode of coke formation (Several reaction: alkylation, cyclization and hydrogen transfer could be involved in step 1)[57].

Organic reactants → soluble coke → insoluble coke

This observation could suggests that the soluble coke molecules are therefore intermediates in the formation of insoluble coke, but the problem with this view is that the hydrocarbons are thought to occupy the cages inside the catalyst and SAPO_34 cages does not have enough space for the compounds bigger than pyrene to be formed. Possible explanations are that the compounds within the cage decomposed with time and then reacted with the coke on the surface of the catalyst, that big compounds connected through the windows forming bigger compounds or that the compounds became insoluble for other reasons, for instance further dehydrogenation.

3.3.2 Determination of coke components

Generally establishing the composition of the insoluble fraction of coke, which consists of highly polyaromatic species is not possible and very often the characterization is limited to the elemental composition. However there are some characterization techniques such as matrix-assisted laser desorption/ionization time-of-flight mass spectrometry (MALDI-TOF MS) and transmission electron microscopy (TEM) coupled with electron energy loss spectroscopy (EELS) which was applied, but Regrettably, the techniques used for insoluble coke analysis are not very practical and, moreover, in contrast to those used for soluble coke analysis, they give only incomplete information on composition[55].

The composition of soluble retained hydrocarbon species in the catalyst at different coke content and temperature of 673 K is shown in Figure 21. These figures show the soluble part of coke consist of polycyclic aromatic, with Di-aromatic, Tricyclic aromatic (Phenanthrene and Anthracene) and Tetracyclic aromatic (Pyrene) as the main constituents. A comparison between the parts (a) and (b) reveals that the aromaticity of the soluble coke increases with the coke content. Figure 22 shows the relative distribution of two-, three, and four- rings in deactivated in the deactivated SAPO_34 at different temperature. As it shown, four-ring aromatic (pyrene) was the major retained organic component and its relative mass fraction increases by temperature. Although the soluble part of coke has the same poly-cyclic aromatic species, but Figure 23 demonstrates different color for partial and complete deactivated SAPO_34. As it shown, deactivated samples at 643, 673, 703 and 733 represent brown, dark brown, black and inky black respectively. By increasing coke content (or increasing TOS) at constant temperature, the color

of samples become darker which demonstrates the relative distribution between soluble and insoluble coke shifted toward heavier species. As previously discussed, these insoluble species cannot be formed through the growth of soluble coke molecules trapped in the pores and cavities of SAPO_34 because the cage of SAPO_34 is so small (the pore structure of SAPO_34 consists of elongated cages (1.1 nm×0.65 nm) linked via relatively small eight-ring intercage windows (3.8 × 3.8 nm)) that it can hardly contain molecular larger than Tetracyclic aromatic. We guess there are insoluble coke species which are formed on the outer surface of SAPO_34 crystals and results in the pore blockage, making internal region of the crystals less accessible to the reactant molecules. It can be understand by the colors of these insoluble coke that, different temperatures results in different insoluble coke species. Aguayo et al. extraction with pyridine has proved the presence of polyaromatics of up to four rings, which are derivatives of pyrene with a molecular weight of up to 400 [58].

3.4 Formulation of coke deposition model

Since the systematic experimental data obtained in present work was under the industrial condition, the conversion was high and the reactor should be treated as an integral plug-flow reactor instead of a differential reactor. Therefore, a distribution of coke is expected and it is reasonable that the coke data is the average content deposited along the reactor.

Applying Matlab2014 curve fitting of the coke data, it was found that coke formation at each different initial condition during MTO reaction is well described through the following exponential function of time.

$$C = (a.e^{b.t} + c.e^{d.t}) \quad (1)$$

Based on our finding, different initial reaction condition resulted in variation of model parameters. Thus, in order to involve the effects of temperature and WHSV in the model, a function of initial condition should be considered.

So the coke model is defined as below,

$$C = H(F(t), G(T, WHSV)) \quad (2)$$

In which F (t) is

$$F(t) = (a.e^{b.t} - c.e^{d.t}) \quad (3)$$

As aforementioned, $F(t)$ has a well description of coke deposition at the initial reaction conditions studied here suggesting the equation constants depend on temperature and weight hour space velocity. In this regards, different functions have been tried to describe the change in coke content with T and WHSV. $G1(T, WHSV)$ And $G2(T, WHSV)$functions were found to give the best fit to the experimental data.

$$G1(T, WHSV) = \left\{ \alpha \left(\frac{T}{1000} \right) + \beta \left(\frac{WHSV}{10} \right) \right\} \quad (4)$$

$$G2(T, WHSV) = \left\{ \left(\frac{T}{1000} \right)^{\alpha} + \left(\frac{WHSV}{10} \right)^{\beta} \right\} \quad (5)$$

Various combination of F (t) and G (T, WHSV) has been tested and finally the following function was found to be a well description of coke deposition behavior.

$$C = \left\{ A \left(\frac{T}{1000} \right) + B \left(\frac{WHSV}{10} \right) \right\} \left(e^{C.\left\{ \left(\left(\frac{T}{1000} \right)^{E} \right) + \left(\left(\frac{WHSV}{10} \right)^{F} \right) \right\}.t} - e^{D.\left\{ \left(\left(\frac{T}{1000} \right)^{G} \right) + \left(\left(\frac{WHSV}{10} \right)^{H} \right) \right\}.t} \right) \quad (6)$$

3.4.1 Model parameters estimation and validation

The coke deposition model Parameters of best fit and their confidence intervals have been determined by particle swarm optimization using MATLAB (2014a, the MathWorks).

Particle swarm optimization is a population-based stochastic optimization method. PSO is first introduced by Eberhart and Kennedy in 1995[59], inspired by social behavior of bird flocking and used for optimization of continuous non-linear functions. It is similar to other population-based evolutionary algorithms in which the algorithm is initialized with a population of random solutions, such as the Ant Colony Optimization (ACO) and GA[60].

In the PSO algorithm, each bird (particle) represents a candidate solution to the optimization problem. In the first step of PSO, initial population of particles are randomly set into motion through the search space. During each iteration, any particle in the population evaluate the fitness values of itself and other particles then adjust its position. (Flowchart of this optimization algorithm is represented in Figure 24 and its general steps is described).

Optimization has been carried out by minimizing an objective function, Φ, which is known as the root mean square error (RMSE) established as the root of Mean Square Error. The RMSE is defined as,

$$RMSE = \sqrt{\frac{1}{N}\sum_{i=1}^{N}(y_i^{exp} - y_i^{cal})^2} \quad (7)$$

Correlation coefficient of predicted and experimental data is also used to measure the accuracy of proposed coke model.

The value of correlation coefficient (CC) is given by,

$$CC = \frac{\sum_{i=1}^{N}(\hat{y}_i - \hat{y})(y_i - \bar{y})}{\sqrt{\sum_{i=1}^{N}(\hat{y}_i - \hat{y})^2(y_i - \bar{y})^2}} \quad (8)$$

Where $\bar{y}$ and $\hat{y}$ are the mean experimental and predicted coke data.

Table 2 and Table 3 shows the validation parameters and the values of calculated model parameters of best fit respectively. The validity of coke deposition model is shown by comparing the experimental (point) and model predicted (line) of evolution of coke content with time on stream in Figure 25.

4 Conclusion

Combined measurement of products selectivity with coke deposition during methanol conversion over the SAPO_34 catalyst at different conditions provides a good macro-model to describe the complex relationship among them. Coke formation proceeded through two stage. A fast increase at lower time on stream and then followed by decreasing rate with a slow increase in carbon material content of catalyst till complete deactivation. Shape selective effect of coke formation shift the product selectivity toward smaller hydrocarbon. Depend on reaction condition, 14wt% to 23wt% coke content of catalyst bed is suggested to be an appropriate range in terms of light olefins production. Reaction temperature and coke content of catalyst bed are found to have a great effect on the formation of coke species. Analysis of coked samples revealed that, by increasing temperature and as the time on stream went on, relative distribution of soluble/insoluble coke shifted towards the heavier component. Depends on the species formed at different reaction temperature, these coke species removal by air treatment varies between the temperature ranges of 550–930 K. Based on the data obtained in this work, a mathematical relation between the initial reaction condition and time on stream with average coke content is proposed as deactivation model.

References

[1] A. T. Aguayo, D. Mier, A. G. Gayubo, M. Gamero, and J. Bilbao, "Kinetics of methanol transformation into hydrocarbons on a HZSM-5 zeolite catalyst at high temperature (400− 550 C)," *Industrial & Engineering Chemistry Research,* vol. 49, pp. 12371-12378, 2010.

[2] J. W. Park, S. J. Kim, M. Seo, S. Y. Kim, Y. Sugi, and G. Seo, "Product selectivity and catalytic deactivation of MOR zeolites with different acid site densities in methanol-to-olefin (MTO) reactions," *Applied Catalysis A: General,* vol. 349, pp. 76-85, 2008.

[3] M. Castro, S. J. Warrender, P. A. Wright, D. C. Apperley, Y. Belmabkhout, G. Pirngruber*, et al.*, "Silicoaluminophosphate molecular sieves STA-7 and STA-14 and their structure-dependent catalytic performance in the conversion of methanol to olefins," *The Journal of Physical Chemistry C,* vol. 113, pp. 15731-15741, 2009.

[4] J. H. Lee, M. B. Park, J. K. Lee, H.-K. Min, M. K. Song, and S. B. Hong, "Synthesis and characterization of ERI-type UZM-12 zeolites and their methanol-to-olefin performance," *Journal of the American Chemical Society,* vol. 132, pp. 12971-12982, 2010.

[5] Q. Wang, Z.-M. Cui, C.-Y. Cao, and W.-G. Song, "0.3 Å makes the difference: dramatic changes in methanol-to-olefin activities between H-ZSM-12 and H-ZSM-22 zeolites," *The Journal of Physical Chemistry C,* vol. 115, pp. 24987-24992, 2011.

[6] S. Teketel, W. Skistad, S. Benard, U. Olsbye, K. P. Lillerud, P. Beato*, et al.*, "Shape selectivity in the conversion of methanol to hydrocarbons: the catalytic performance of one-dimensional 10-ring zeolites: ZSM-22, ZSM-23, ZSM-48, and EU-1," *ACS Catalysis,* vol. 2, pp. 26-37, 2011.

[7] Y. Bhawe, M. Moliner-Marin, J. D. Lunn, Y. Liu, A. Malek, and M. Davis, "Effect of cage size on the selective conversion of methanol to light olefins," *Acs Catalysis,* vol. 2, pp. 2490-2495, 2012.

[8] M.-A. Djieugoue, A. Prakash, and L. Kevan, "Catalytic study of methanol-to-olefins conversion in four small-pore silicoaluminophosphate molecular sieves: influence of the structural type, nickel incorporation, nickel location, and nickel concentration," *The Journal of Physical Chemistry B,* vol. 104, pp. 6452-6461, 2000.

[9] S. Svelle, U. Olsbye, F. Joensen, and M. Bjørgen, "Conversion of methanol to alkenes over medium-and large-pore acidic zeolites: Steric manipulation of the reaction intermediates governs the ethene/propene product selectivity," *The Journal of Physical Chemistry C,* vol. 111, pp. 17981-17984, 2007.

[10] J. Q. Chen, A. Bozzano, B. Glover, T. Fuglerud, and S. Kvisle, "Recent advancements in ethylene and propylene production using the UOP/Hydro MTO process," *Catalysis today,* vol. 106, pp. 103-107, 2005.

[11] G. Yang, Y. Wei, S. Xu, J. Chen, J. Li, Z. Liu, *et al.*, "Nanosize-enhanced lifetime of SAPO-34 catalysts in methanol-to-olefin reactions," *The Journal of Physical Chemistry C,* vol. 117, pp. 8214-8222, 2013.

[12] C. Wang, M. Yang, P. Tian, S. Xu, Y. Yang, D. Wang, *et al.*, "Dual template-directed synthesis of SAPO-34 nanosheet assemblies with improved stability in the methanol to olefins reaction," *Journal of Materials Chemistry A,* 2015.

[13] B. Vora, T. Marker, E. Arnold, H. Nilsen, S. Kvisle, and T. Fuglerud, "Conversion of natural gas to ethylene and propylene: The most-profitable option," *Studies in surface science and catalysis,* pp. 955-960, 1998.

[14] N. Nishiyama, M. Kawaguchi, Y. Hirota, D. Van Vu, Y. Egashira, and K. Ueyama, "Size control of SAPO-34 crystals and their catalyst lifetime in the methanol-to-olefin reaction," *Applied Catalysis A: General,* vol. 362, pp. 193-199, 2009.

[15] D. Chen, K. Moljord, T. Fuglerud, and A. Holmen, "The effect of crystal size of SAPO-34 on the selectivity and deactivation of the MTO reaction," *Microporous and Mesoporous Materials,* vol. 29, pp. 191-203, 1999.

[16] Q. Sun, Y. Ma, N. Wang, X. Li, D. Xi, J. Xu, *et al.*, "High performance nanosheet-like silicoaluminophosphate molecular sieves: synthesis, 3D EDT structural analysis and MTO catalytic studies," *Journal of Materials Chemistry A,* vol. 2, pp. 17828-17839, 2014.

[17] W. Dai, C. Wang, M. Dyballa, G. Wu, N. Guan, L. Li, *et al.*, "Understanding the early stages of the methanol-to-olefin conversion on H-SAPO-34," *ACS Catalysis,* vol. 5, pp. 317-326, 2014.

[18] W. Dai, M. Dyballa, G. Wu, L. Li, N. Guan, and M. Hunger, "Intermediates and Dominating Reaction Mechanism During the Early Period of the Methanol-to-Olefin Conversion on SAPO-41," *The Journal of Physical Chemistry C,* vol. 119, pp. 2637-2645, 2015.

[19] K. De Wispelaere, K. Hemelsoet, M. Waroquier, and V. Van Speybroeck, "Complete low-barrier side-chain route for olefin formation during methanol conversion in H-SAPO-34," *Journal of Catalysis,* vol. 305, pp. 76-80, 2013.

[20] C.-M. Wang, Y.-D. Wang, and Z.-K. Xie, "Insights into the reaction mechanism of methanol-to-olefins conversion in HSAPO-34 from first principles: Are olefins themselves the dominating hydrocarbon pool species?," *Journal of Catalysis,* vol. 301, pp. 8-19, 2013.

[21] S. Ilias and A. Bhan, "Mechanism of the catalytic conversion of methanol to hydrocarbons," *ACS Catalysis,* vol. 3, pp. 18-31, 2012.

[22] Y.-J. Lee, S.-C. Baek, and K.-W. Jun, "Methanol conversion on SAPO-34 catalysts prepared by mixed template method," *Applied Catalysis A: General,* vol. 329, pp. 130-136, 2007.

[23] M. Stöcker, "Methanol-to-hydrocarbons: catalytic materials and their behavior," *Microporous and Mesoporous Materials,* vol. 29, pp. 3-48, 1999.

[24] J. Chen, J. Li, C. Yuan, S. Xu, Y. Wei, Q. Wang*, et al.*, "Elucidating the olefin formation mechanism in the methanol to olefin reaction over AlPO-18 and SAPO-18," *Catalysis Science & Technology,* vol. 4, pp. 3268-3277, 2014.

[25] W. Song, H. Fu, and J. F. Haw, "Supramolecular origins of product selectivity for methanol-to-olefin catalysis on HSAPO-34," *Journal of the American Chemical Society,* vol. 123, pp. 4749-4754, 2001.

[26] M. Bjørgen, U. Olsbye, and S. Kolboe, "Coke precursor formation and zeolite deactivation: mechanistic insights from hexamethylbenzene conversion," *Journal of Catalysis,* vol. 215, pp. 30-44, 2003.

[27] U. Olsbye, S. Svelle, M. Bjørgen, P. Beato, T. V. Janssens, F. Joensen*, et al.*, "Conversion of methanol to hydrocarbons: how zeolite cavity and pore size controls product selectivity," *Angewandte Chemie International Edition,* vol. 51, pp. 5810-5831, 2012.

[28] S. M. Alwahabi and G. F. Froment, "Single event kinetic modeling of the methanol-to-olefins process on SAPO-34," *Industrial & engineering chemistry research,* vol. 43, pp. 5098-5111, 2004.

[29] D. Chen, H. Rebo, A. Grønvold, K. Moljord, and A. Holmen, "Methanol conversion to light olefins over SAPO-34: kinetic modeling of coke formation," *Microporous and Mesoporous Materials,* vol. 35, pp. 121-135, 2000.

[30] O. Levenspiel, "Chemical reaction engineering," *Industrial & engineering chemistry research,* vol. 38, pp. 4140-4143, 1999.

[31] T. V. Janssens, S. Svelle, and U. Olsbye, "Kinetic modeling of deactivation profiles in the methanol-to-hydrocarbons (MTH) reaction: A combined autocatalytic–hydrocarbon pool approach," *Journal of Catalysis,* vol. 308, pp. 122-130, 2013.

[32] M. Guisnet and F. R. Ribeiro, *Deactivation and regeneration of zeolite catalysts* vol. 9: World Scientific Singapore, 2011.

[33] B. P. Hereijgers, F. Bleken, M. H. Nilsen, S. Svelle, K.-P. Lillerud, M. Bjørgen*, et al.*, "Product shape selectivity dominates the Methanol-to-Olefins (MTO) reaction over H-SAPO-34 catalysts," *Journal of catalysis,* vol. 264, pp. 77-87, 2009.

[34] B. Lok, C. Messina, R. Patton, R. Gajek, T. Cannon, and E. FLANIGEN, "Crystalline silicoaluminophosphates: US, 4440871," ed, 1984.

[35] R. M. Behbahani, R. B. Rostami, and A. S. Lemraski, "Methanol/dimethyl ether to light olefins over SAPO-34: Comprehensive comparison of the products distribution and catalyst performance," *Journal of Natural Gas Science and Engineering,* vol. 21, pp. 532-539, 2014.

[36] S. Hajimirzaee, G. A. Leeke, and J. Wood, "Modified zeolite catalyst for selective dialkylation of naphthalene," *Chemical Engineering Journal,* vol. 207, pp. 329-341, 2012.

[37] A. T. Aguayo, A. G. Gayubo, J. Ereña, M. Olazar, J. M. Arandes, and J. Bilbao, "Isotherms of chemical adsorption of bases on solid catalysts for acidity measurement," *Journal of Chemical Technology and Biotechnology,* vol. 60, pp. 141-146, 1994.

[38] B. Parlitz, E. Schreier, H. Zubowa, R. Eckelt, E. Lieske, G. Lischke*, et al.*, "Isomerization of n-heptane over Pd-loaded silico-alumino-phosphate molecular sieves," *Journal of Catalysis,* vol. 155, pp. 1-11, 1995.

[39] D. Chen, K. Moljord, and A. Holmen, "A methanol to olefins review: Diffusion, coke formation and deactivation on SAPO type catalysts," *Microporous and mesoporous materials,* vol. 164, pp. 239-250, 2012.

[40] M. Ghavipour, R. M. Behbahani, G. R. Moradi, and A. Soleimanimehr, "Methanol dehydration over alkali-modified H-ZSM-5; effect of temperature and water dilution on products distribution," *Fuel,* vol. 113, pp. 310-317, 2013.

[41] F. Yaripour, Z. Shariatinia, S. Sahebdelfar, and A. Irandoukht, "Effect of boron incorporation on the structure, products selectivities and lifetime of H-ZSM-5 nanocatalyst designed for application in methanol-to-olefins (MTO) reaction," *Microporous and Mesoporous Materials,* vol. 203, pp. 41-53, 2015.

[42] E. J. Munson, A. A. Kheir, N. D. Lazo, and J. F. Haw, "In situ solid-state NMR study of methanol-to-gasoline chemistry in zeolite HZSM-5," *The Journal of Physical Chemistry,* vol. 96, pp. 7740-7746, 1992.

[43] F. Salehirad and M. W. Anderson, "Solid-State 13 C MAS NMR Study of Methanol-to-Hydrocarbon Chemistry over H-SAPO-34," *Journal of Catalysis,* vol. 164, pp. 301-314, 1996.

[44] G. J. Hutchings and R. Hunter, "Hydrocarbon formation from methanol and dimethyl ether: a review of the experimental observations concerning the mechanism of formation of the primary products," *Catalysis today,* vol. 6, pp. 279-306, 1990.

[45] D. Chen, H. P. Rebo, and A. Holmen, "Diffusion and deactivation during methanol conversion over SAPO-34: a percolation approach," *Chemical engineering science,* vol. 54, pp. 3465-3473, 1999.

[46] P. Tian, Y. Wei, M. Ye, and Z. M. Liu, "Methanol to Olefins (MTO): From Fundamentals to Commercialization," *ACS Catalysis,* vol. 5, pp. 1922-1938, 2015.

[47] S. Teketel, M. W. Erichsen, F. L. Bleken, S. Svelle, and K. Petter, "Shape selectivity in zeolite catalysis–The methanol to hydrocarbons (MTH) reaction," *SPR Catalysis V26,* vol. 26, pp. 179-217, 2014.

[48] J. F. Haw, W. Song, D. M. Marcus, and J. B. Nicholas, "The mechanism of methanol to hydrocarbon catalysis," *Accounts of chemical research,* vol. 36, pp. 317-326, 2003.

[49] P. L. Benito, A. G. Gayubo, A. T. Aguayo, M. Olazar, and J. Bilbao, "Deposition and characteristics of coke over a H-ZSM5 zeolite-based catalyst in the MTG process," *Industrial & engineering chemistry research,* vol. 35, pp. 3991-3998, 1996.

[50] H. Hu, F. Cao, W. Ying, Q. Sun, and D. Fang, "Study of coke behaviour of catalyst during methanol-to-olefins process based on a special TGA reactor," *Chemical Engineering Journal,* vol. 160, pp. 770-778, 2010.

[51] G. Qi, Z. Xie, W. Yang, S. Zhong, H. Liu, C. Zhang*, et al.*, "Behaviors of coke deposition on SAPO-34 catalyst during methanol conversion to light olefins," *Fuel processing technology,* vol. 88, pp. 437-441, 2007.

[52] A. Marchi and G. Froment, "Catalytic conversion of methanol to light alkenes on SAPO molecular sieves," *Applied catalysis,* vol. 71, pp. 139-152, 1991.

[53] X. Wu, M. G. Abraha, and R. G. Anthony, "Methanol conversion on SAPO-34: reaction condition for fixed-bed reactor," *Applied Catalysis A: General,* vol. 260, pp. 63-69, 2004.

[54] Y. Wei, J. Li, C. Yuan, S. Xu, Y. Zhou, J. Chen*, et al.*, "Generation of diamondoid hydrocarbons as confined compounds in SAPO-34 catalyst in the conversion of methanol," *Chemical Communications,* vol. 48, pp. 3082-3084, 2012.

[55] M. Guisnet, L. Costa, and F. R. Ribeiro, "Prevention of zeolite deactivation by coking," *Journal of Molecular Catalysis A: Chemical,* vol. 305, pp. 69-83, 2009.

[56] D. Mores, E. Stavitski, M. H. Kox, J. Kornatowski, U. Olsbye, and B. M. Weckhuysen, "Space-and Time-Resolved In-situ Spectroscopy on the Coke Formation in Molecular Sieves: Methanol-to-Olefin Conversion over H-ZSM-5 and H-SAPO-34," *Chemistry-A European Journal,* vol. 14, pp. 11320-11327, 2008.

[57] M. Guisnet, P. Magnoux, and D. Martin, "Roles of acidity and pore structure in the deactivation of zeolites by carbonaceous deposits," *Studies in surface science and catalysis,* vol. 111, pp. 1-19, 1997.

[58] A. T. Aguayo, A. E. Campo, A. G. Gayubo, A. Tarrío, and J. Bilbao, "Deactivation by coke of a catalyst based on a SAPO-34 in the transformation of methanol into olefins," *Journal of chemical Technology and Biotechnology,* vol. 74, pp. 315-321, 1999.

[59] R. C. Eberhart and J. Kennedy, "A new optimizer using particle swarm theory," in *Proceedings of the sixth international symposium on micro machine and human science*, 1995, pp. 39-43.

[60] D. ping Tian, "A Review of Convergence Analysis of Particle Swarm Optimization," *International Journal of Grid and Distributed Computing,* vol. 6, pp. 117-128, 2013.

Figures

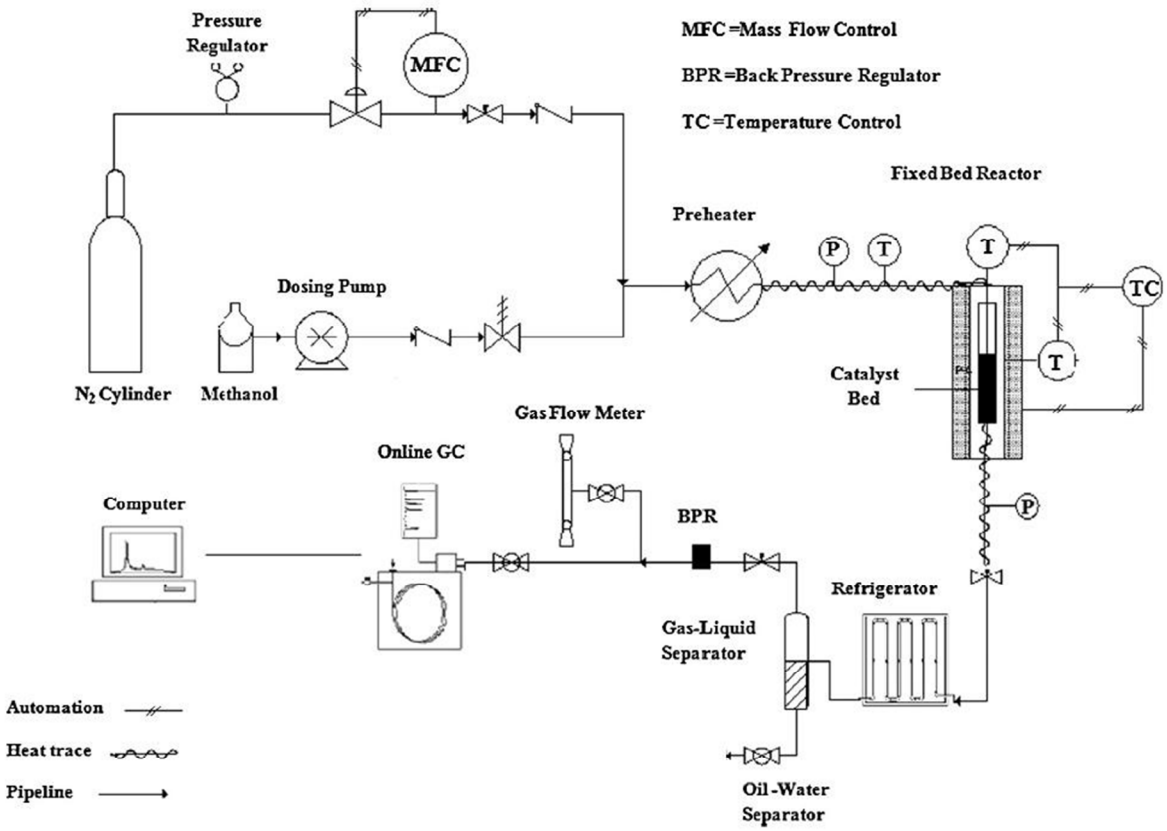

Figure 1. Scheme of the experimental reaction setup.

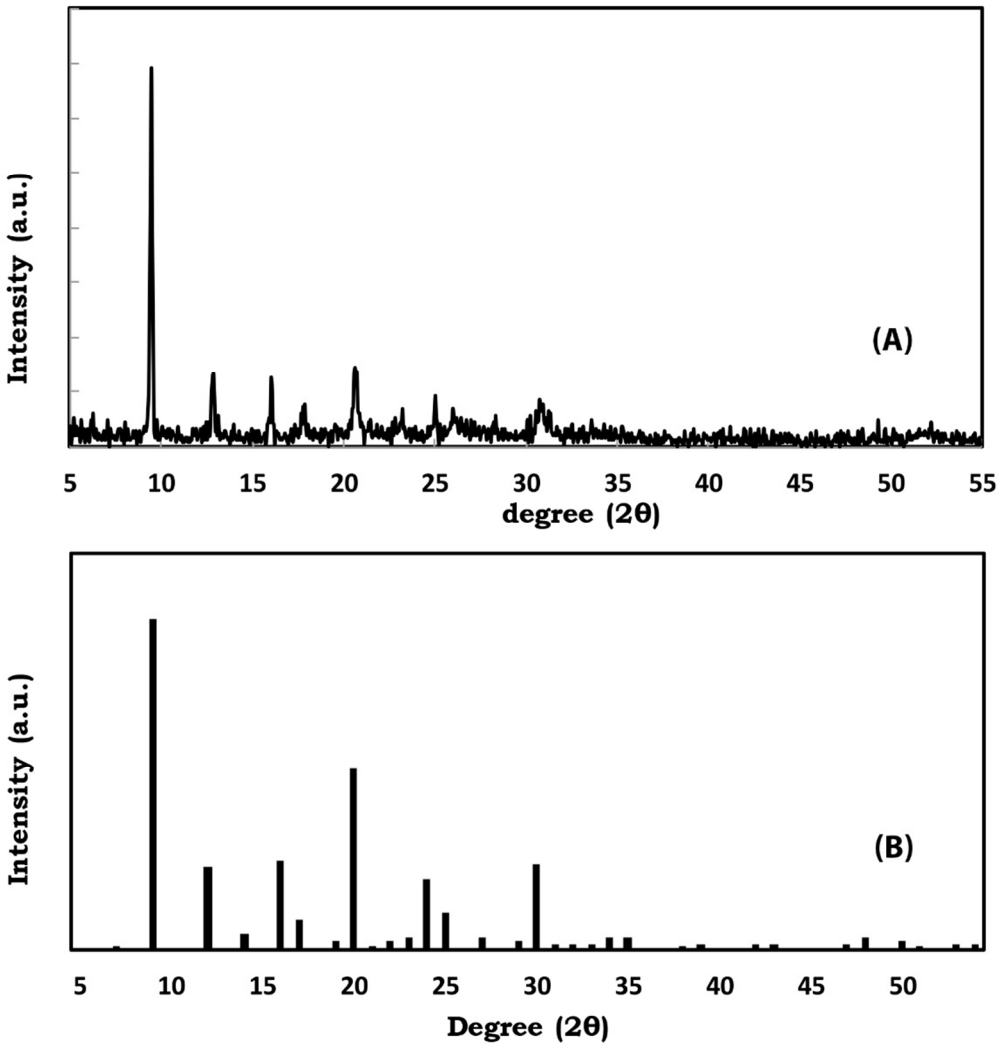

Figure 2. XRD patterns of A) synthesized SAPO_34 fresh catalyst, B) Reference pattern.

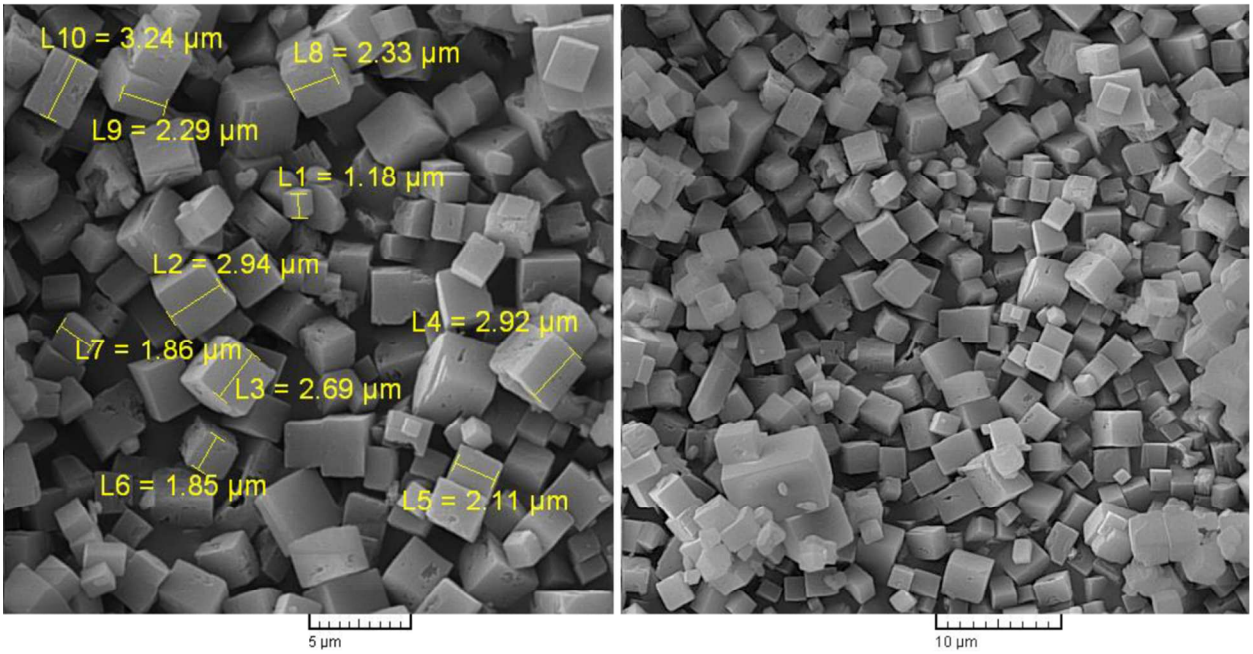

Figure 3. SEM photographs of synthesized SAPO_34 catalyst.

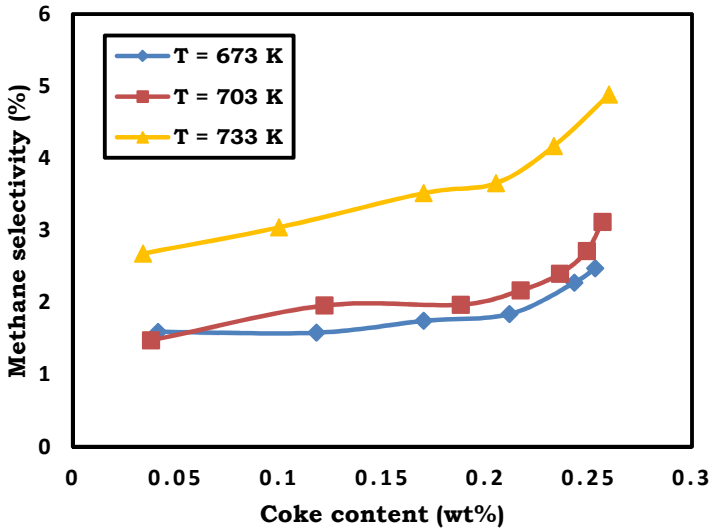

Figure 4. Methane selectivity vs. coke content of SAPO_34 during MTO reaction at WHSV=2 hr^{-1}.

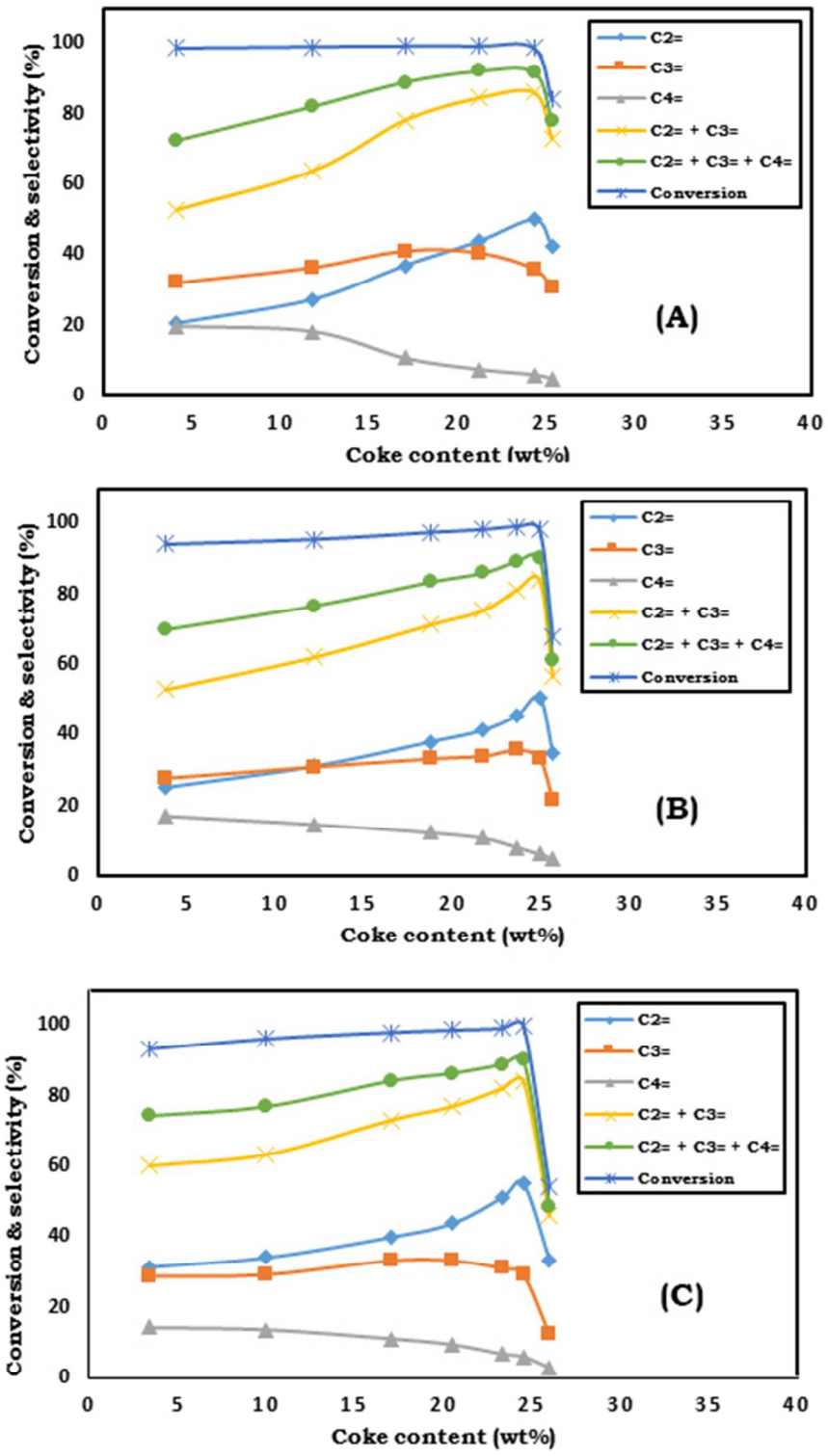

Figure 5. Effect of coke deposition on the methanol conversion and selectivity to light olefins at WHSV = 2 hr-1 and (A, T= 673 K), (B, T= 703 K), (C, T= 733 K).

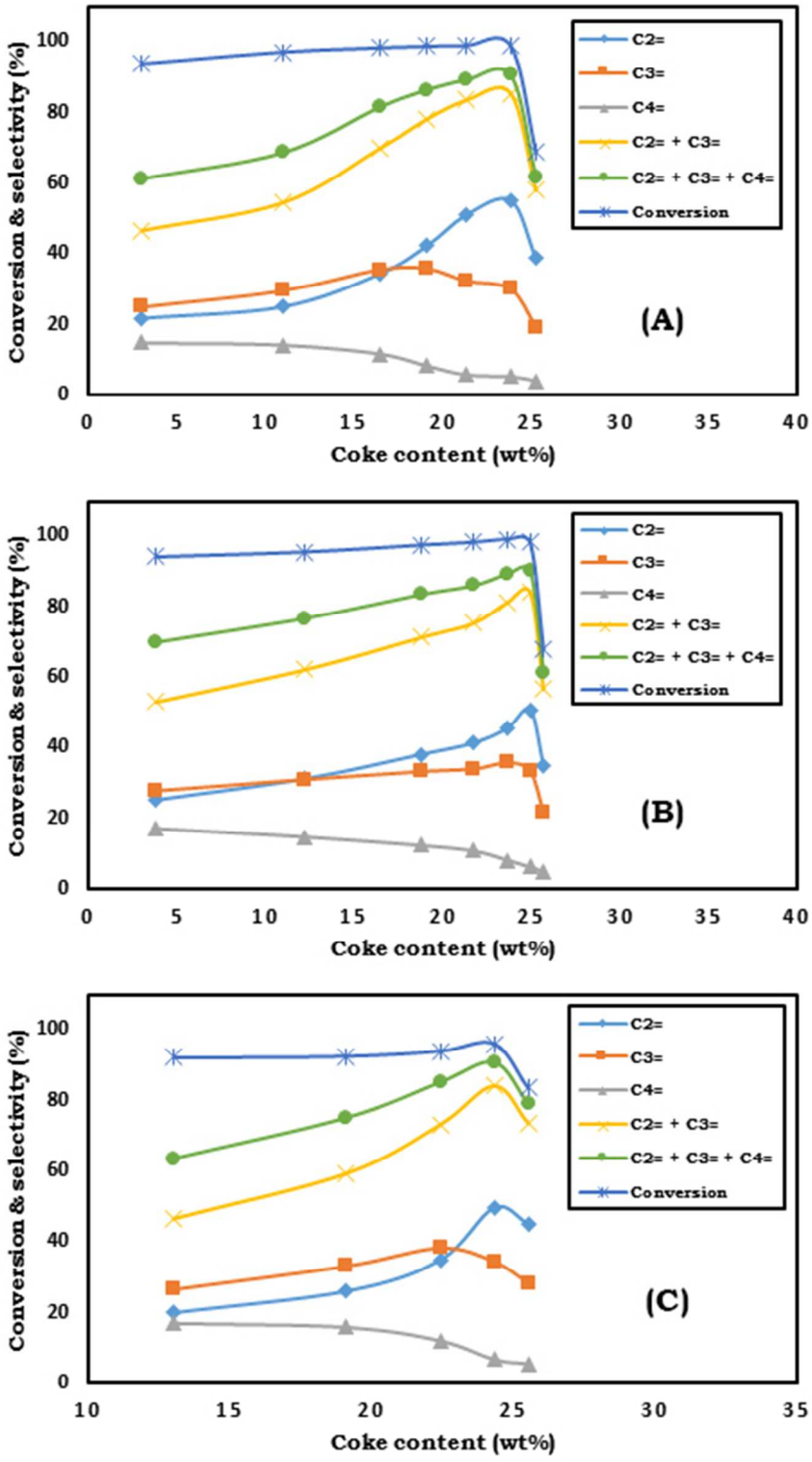

Figure 6. Effect of coke deposition on the methanol conversion and selectivity to light olefins at T=703 K and (A, WHSV = 1 hr-1), (B, WHSV = 2 hr-1), (C, WHSV = 4 hr-1).

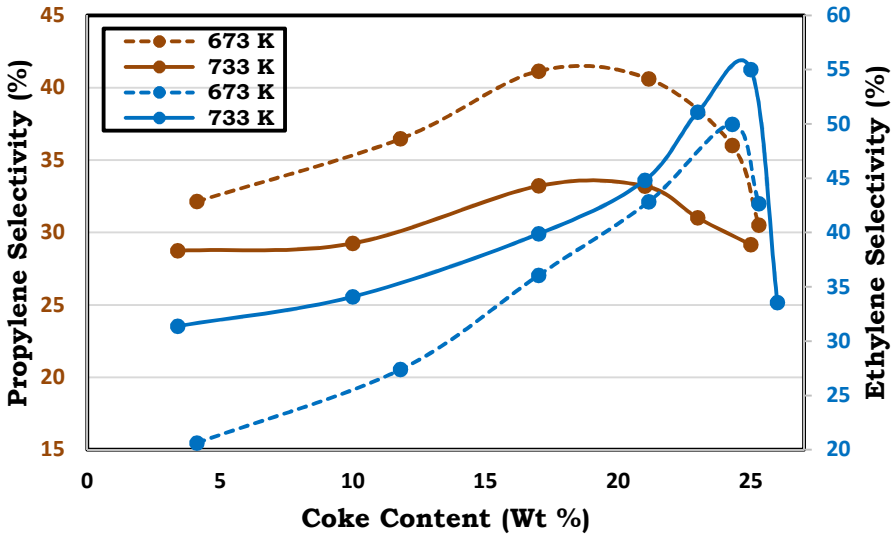

Figure 7. Effect of temperature on Ethylene & Propylene vs. coke content at WHSV = 2 hr^{-1}.

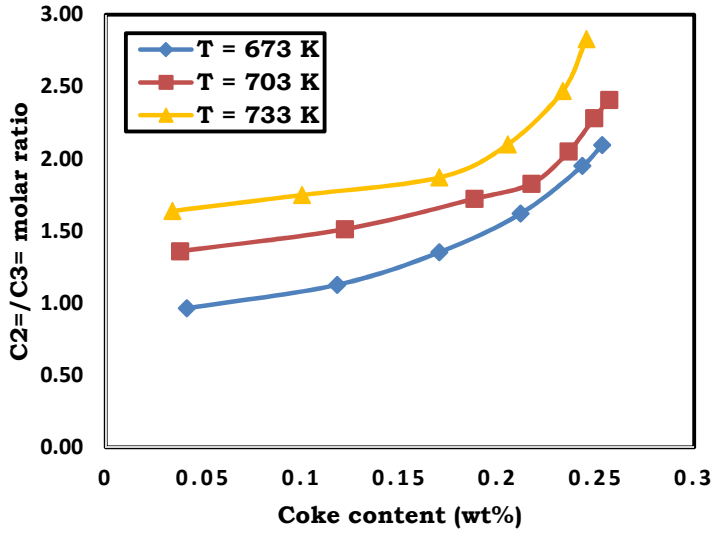

Figure 8. Ethylene to Propylene molar ratio vs. coke content of SAPO_34 during MTO reaction (WHSV = 2 hr^{-1}).

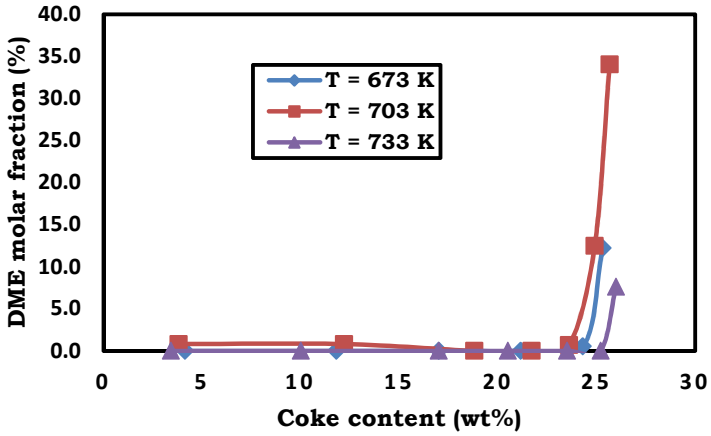

Figure 9. DME mole fraction with different coke content at WHSV=2 hr^{-1}.

Figure 10. C2 & C3 HTI of MTO at T=703 K.

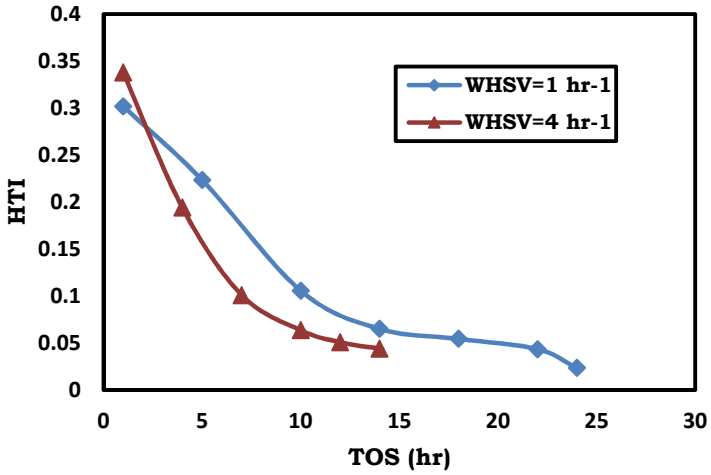
0.4
0.35
0.3
0.25
0.2
0.15
0.1
0.05
0
HTI
0
5
10
15
20
25
30
TOS (hr)
WHSV=1 hr-1
WHSV=4 hr-1

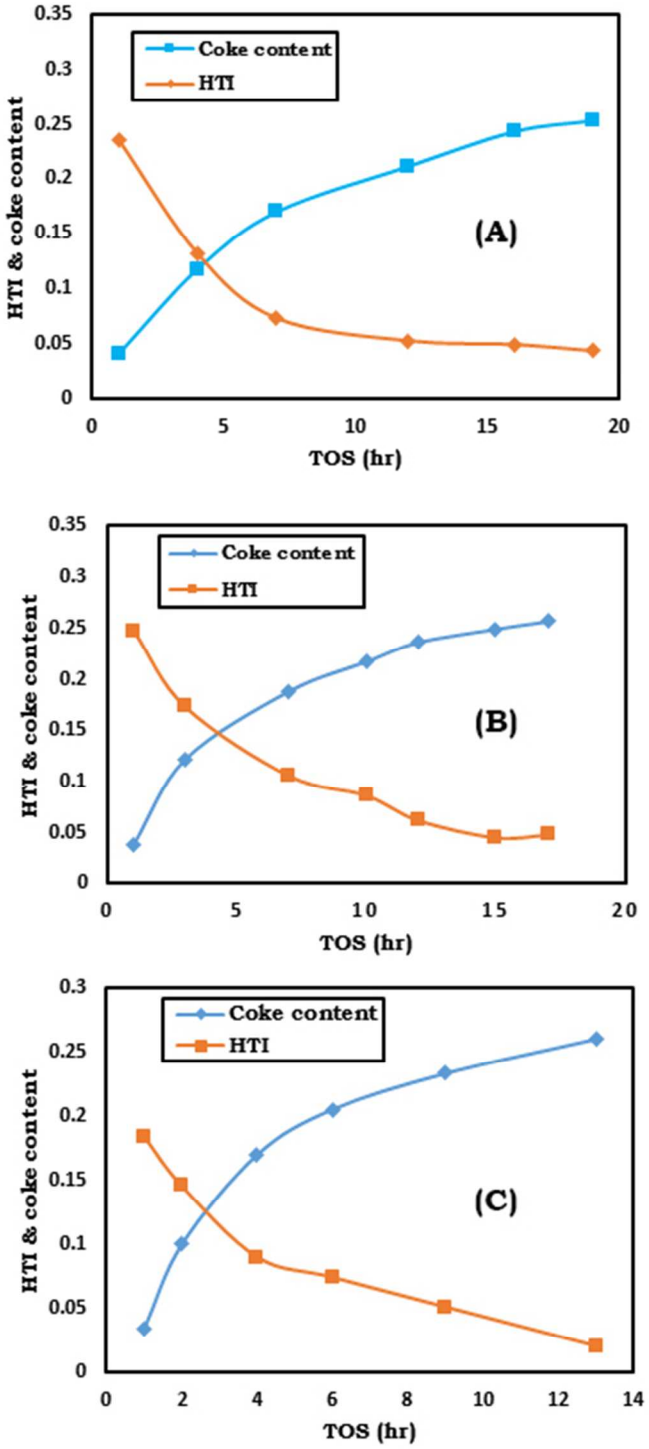

Figure 11. C2 & C3 HTI of MTO at WHSV=2 hr^{-1} (A, T= 673 K), (B, T= 703 K), (C, T= 733 K).

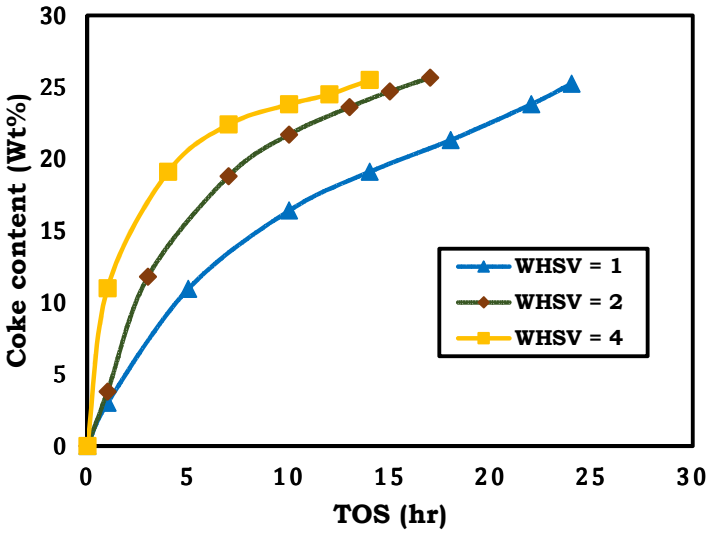

Figure 12. Coke deposition vs. time-on-stream in the MTO reaction catalyzed by SAPO-34. Reaction test conditions: T = 703 K, WHSV = 1, 2, and 4 h^{-1}.

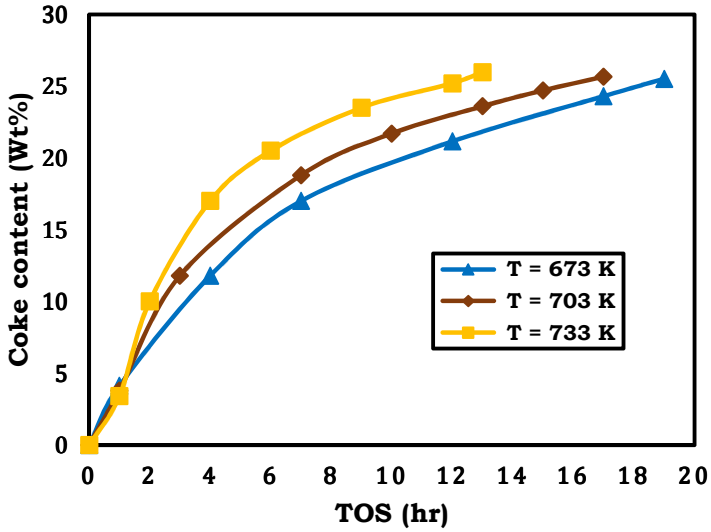

Figure 13. Coke deposition vs. time-on-stream in the MTO reaction catalyzed by SAPO-34. Reaction test conditions: T = 673, 703 and 733 K, WHSV = 2 h^{-1}.

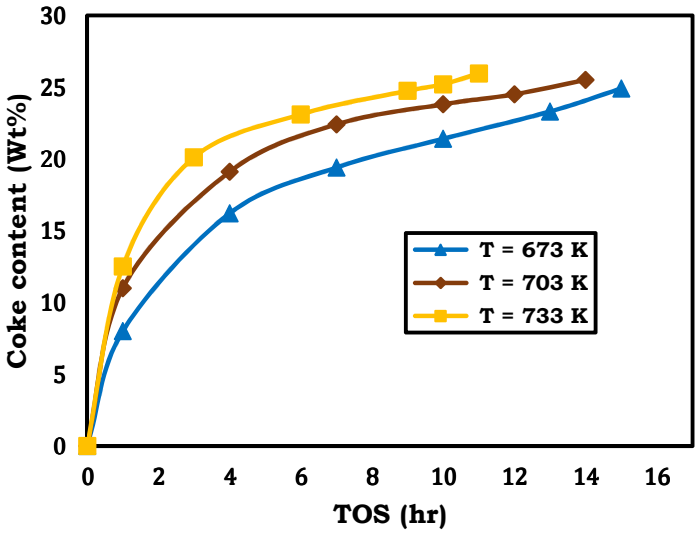

Figure 14. Coke deposition vs. time-on-stream in the MTO reaction catalyzed by SAPO-34. Reaction test conditions: T = 673, 703 and 733 K, WHSV = 4 h^{-1}.

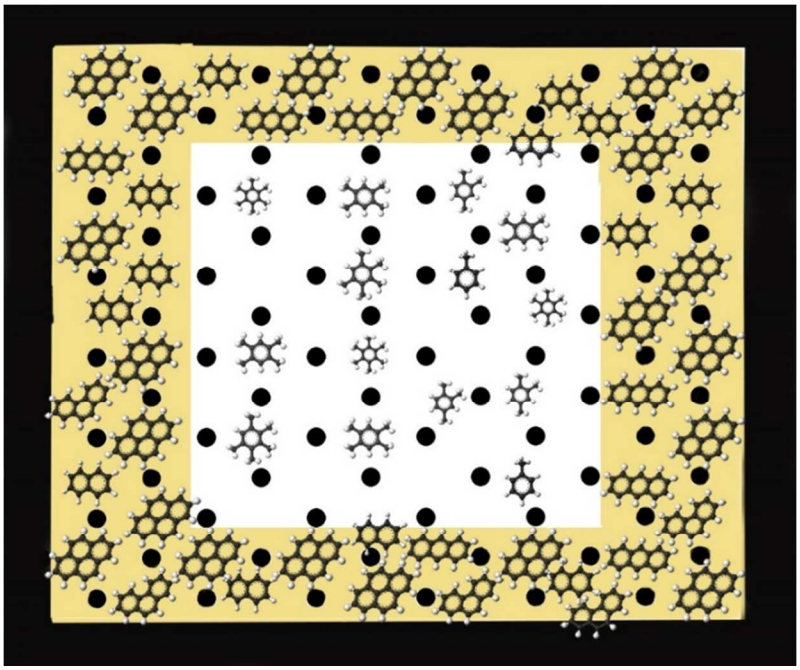

Figure 15. Schematic 2-D cross-sectional representation of deactivated cubic particle of SAPO_34. The black area around the particle represents insoluble coke deposited on the outer surface of catalyst. Brown area represents soluble coke formed in the cages near the outer surface.

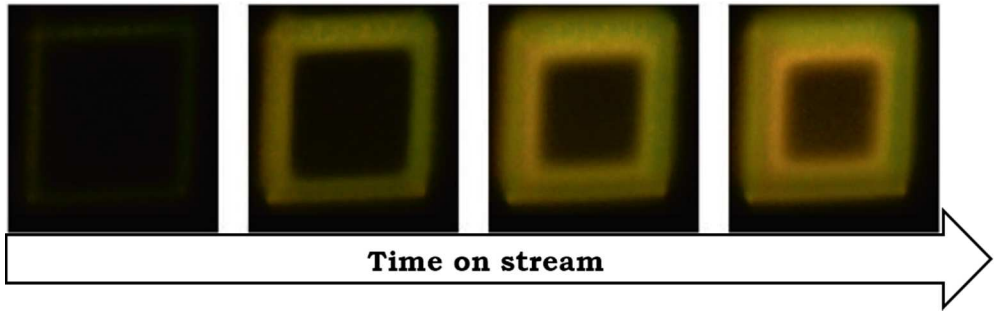

Figure 16. Fluorescence profiles of an individual SAPO-34 crystal during MTO reaction.

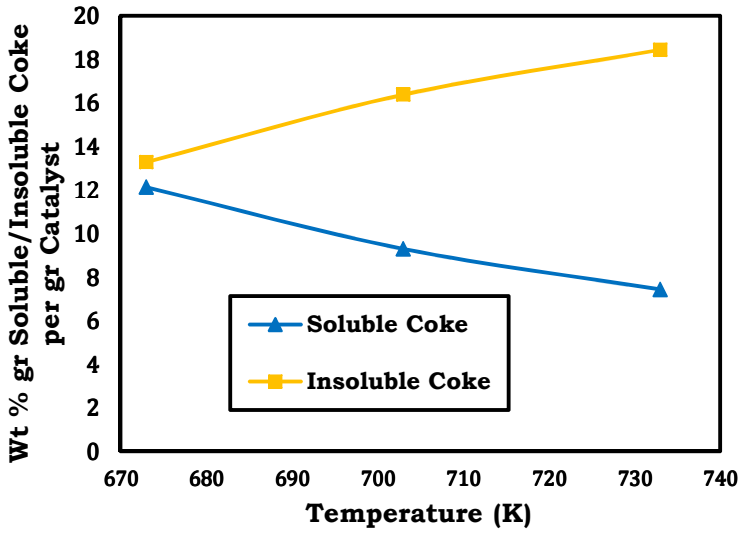

Figure 17. Weight percentage variation of soluble and insoluble coke* species in CH_2Cl_2 deposited on deactivated SAPO_34 as a function of the reaction temperature at WHSV=2 hr^{-1}.

* The total carbon deposited materials are measured by TGA. The soluble part of coke species is calculated by summation of the species quality dissolved in dichloromethane (CH_2Cl_2). Difference between the amount of total carbon deposited material and soluble coke was considered as insoluble coke quality.

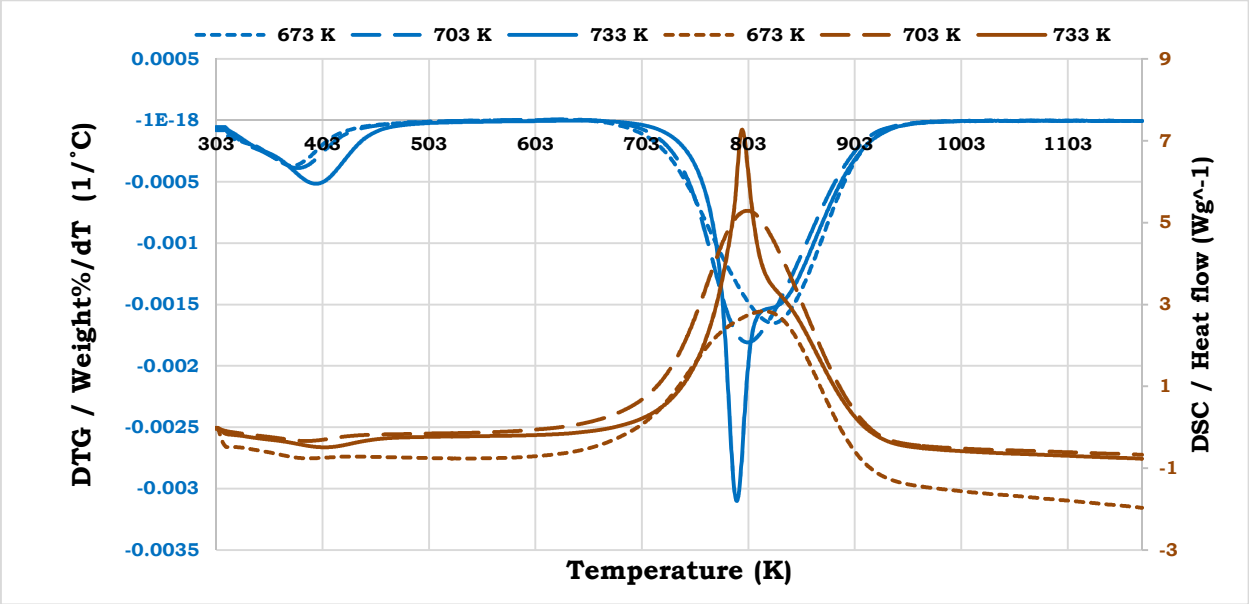

Figure 18. DSC / DTG profiles of deactivated SAPO-34 catalysts at WHSV = 2 hr^{-1} and different reaction temperature.

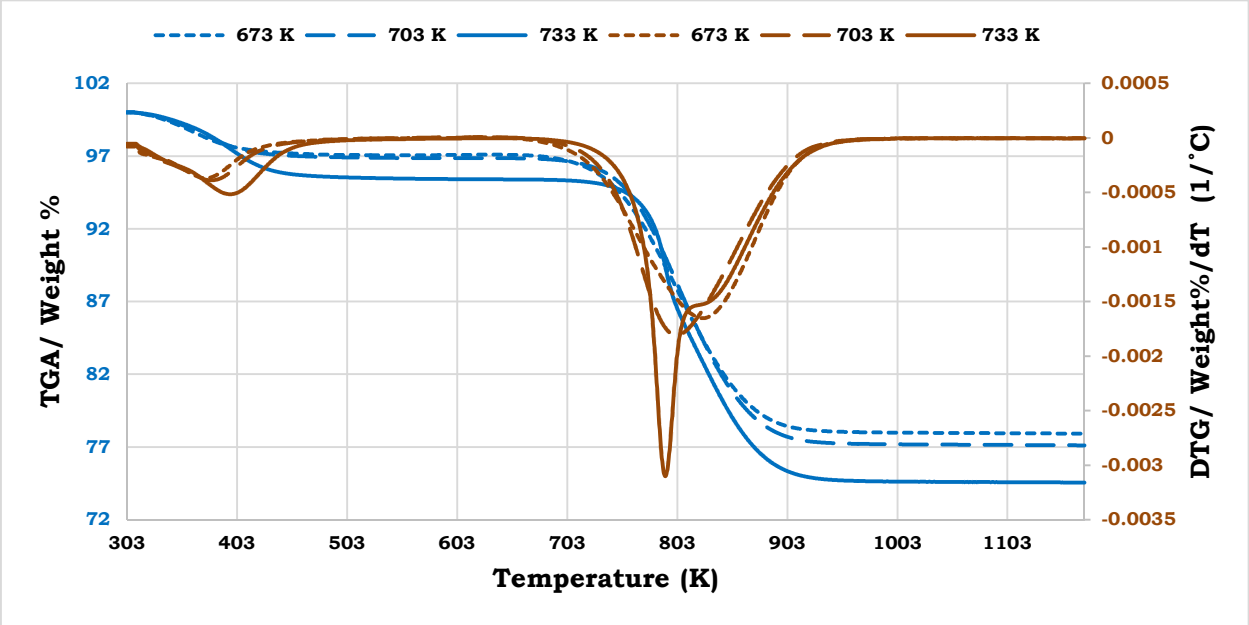

Figure 19. TGA / DTG profiles of deactivated SAPO-34 catalysts at WHSV = 2 hr^{-1} and different reaction temperature.

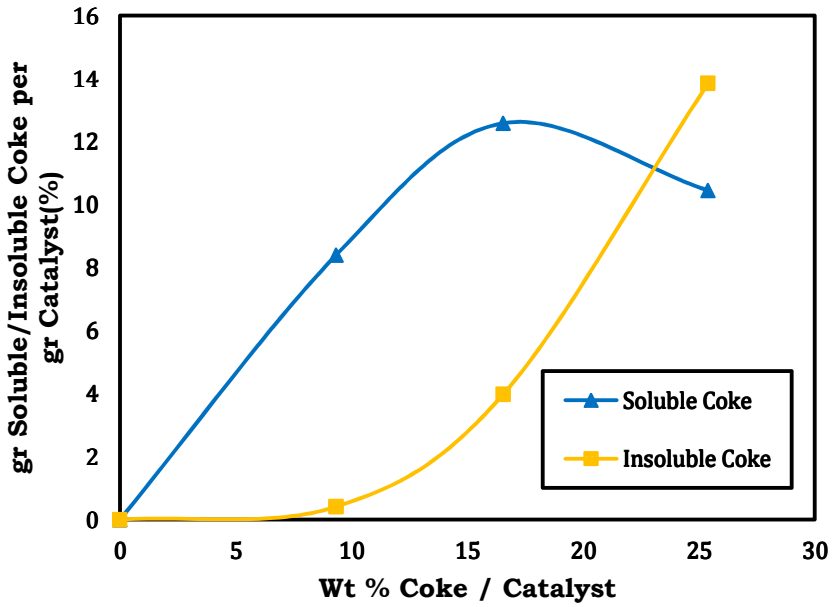

Figure 20. Weight percentage variation of soluble and insoluble coke species in CH_2Cl_2 deposited on deactivated SAPO_34 as a function of the percentage of coke formed during MTO reaction at 703 K.

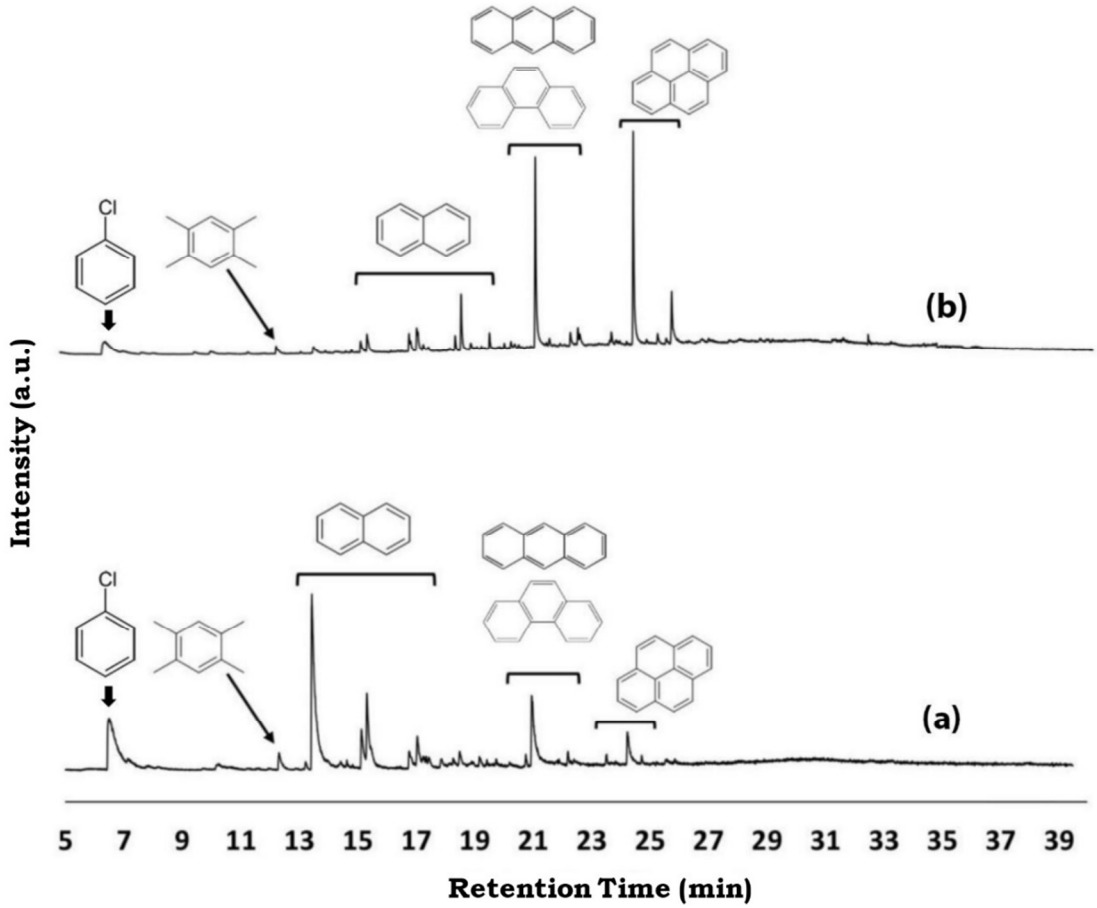

Figure 21. GC-MS analysis of soluble retained organics in the SAPO_34 catalyst at 673 K ((a) 15 Wt% grcoke/gr catalyst and (b) 26 Wt% grcoke/gr catalyst).

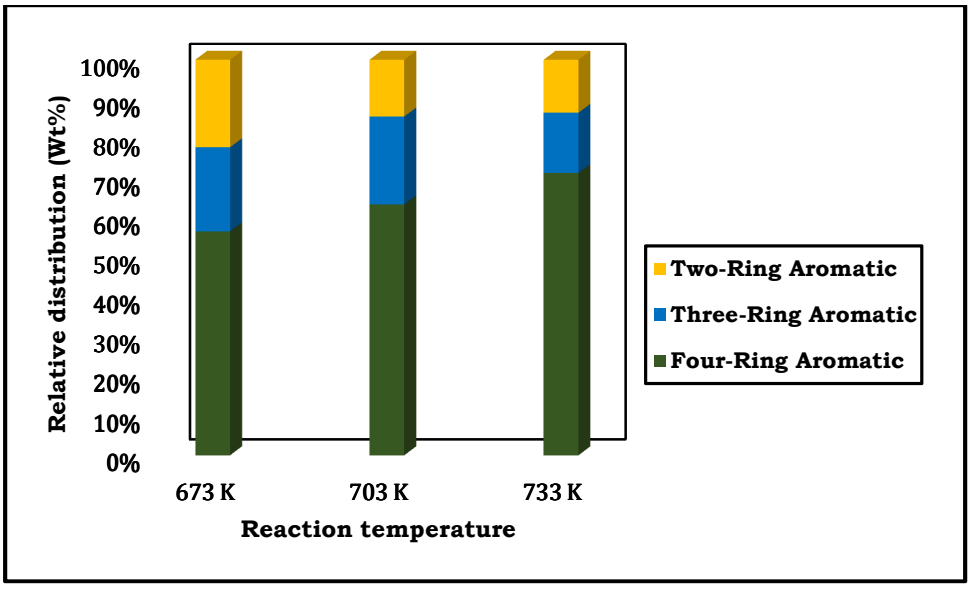

Figure 22. Relative distribution of two-, three, and four- rings aromatic species formed in deactivated SAPO-34 at different reaction temperature.

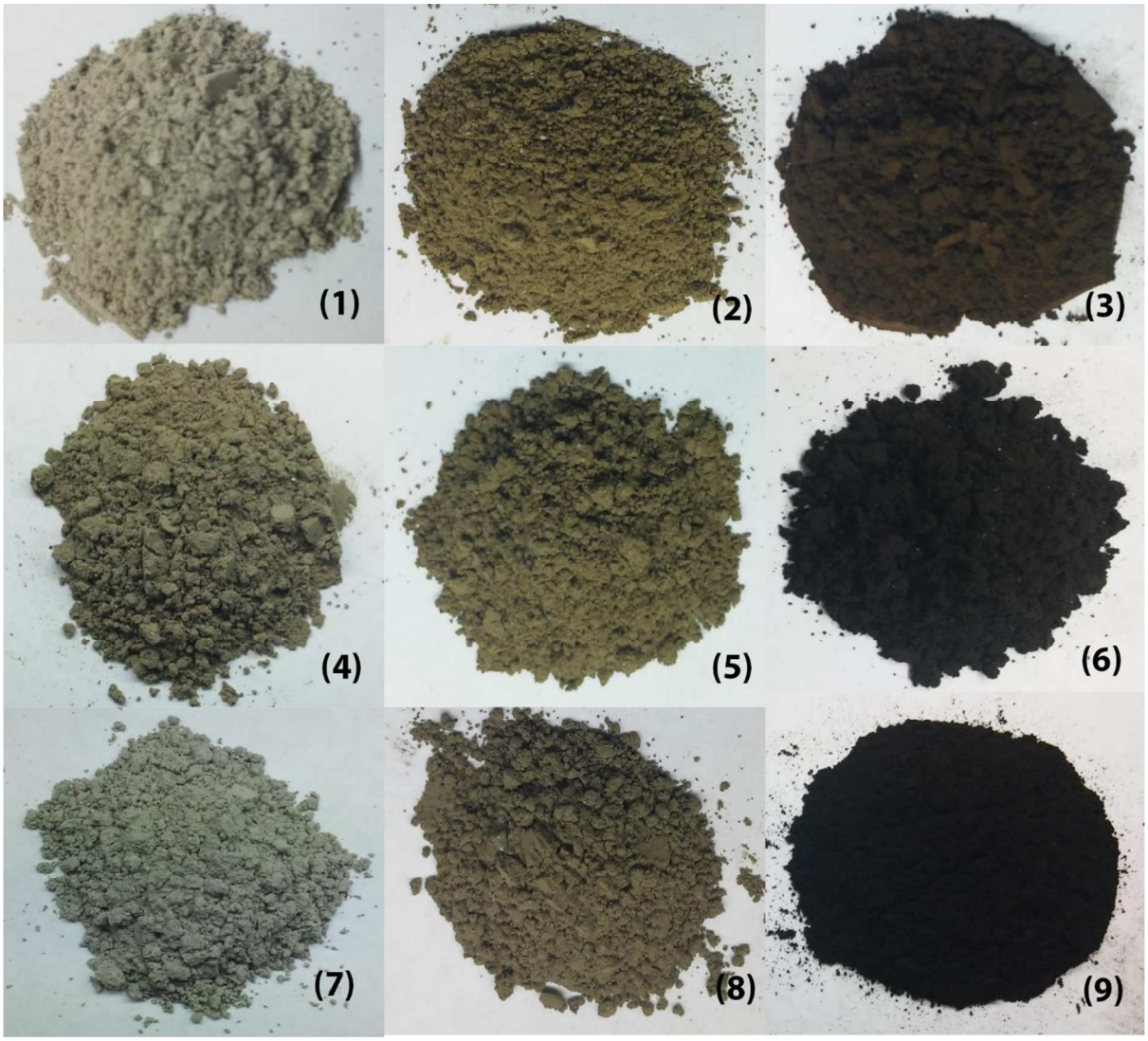

Figure 23. Partial and complete deactivated SAPO_34 samples (After the reaction, the catalysts were flushed for a determined time and cooled down quickly). Samples 3, 6, 9 are complete deactivated SAPO_34 and samples 1, 2, 4, 5, 7, 8 are partial deactivated catalysts.

Sample 3, 6 and 9 were deactivated at 673, 703 and 733 K respectively.

Sample 1 (673 K & 4.13 Wt% coke/ gr catalyst), 2 (673 K & 15.48 Wt% coke/ gr catalyst), 4 (703 K & 6.4 Wt% coke/ gr catalyst), 5 (703 K & 16.55 Wt% coke/ gr catalyst), 7 (733 K & 3.41 Wt% coke/ gr catalyst), 8 (733 K & 9.7 Wt% coke/ gr catalyst).

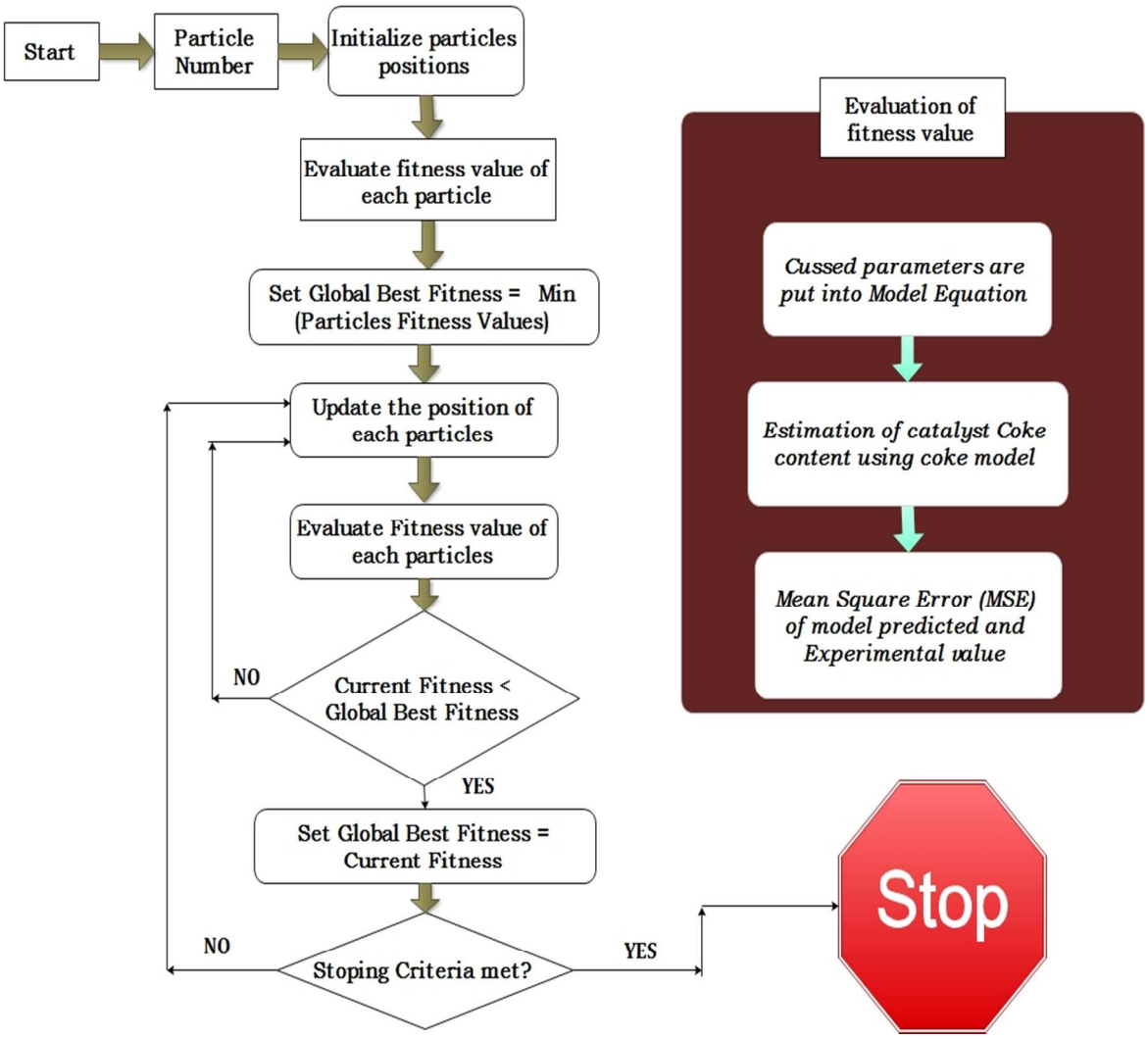

Figure 24. Flowchart of PSO general steps.

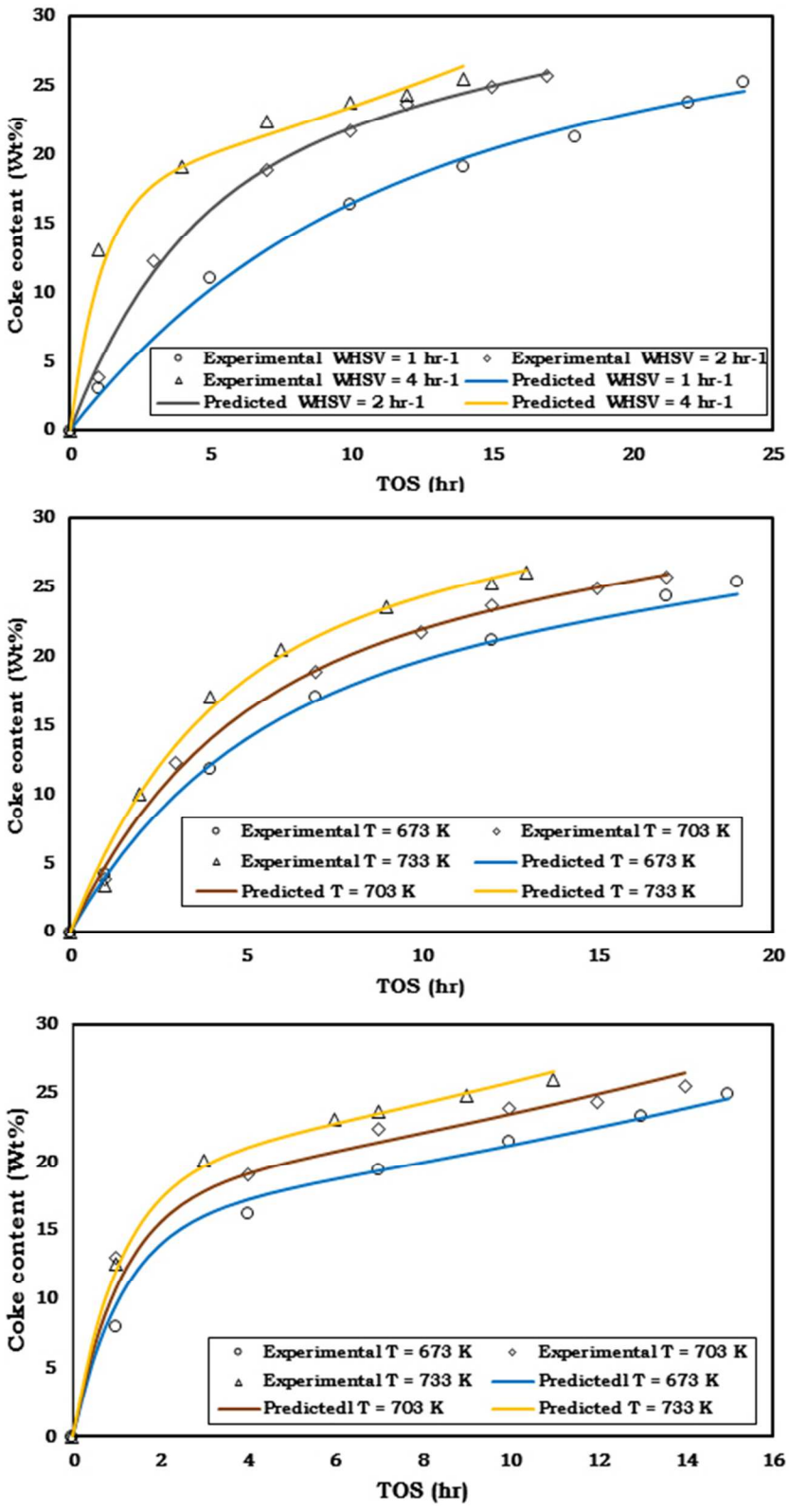

Figure 25. Comparison of calculated coke content with time at different temperature and space velocity according to the proposed model with experimental acquired data using SAPO_34.

Tables

Table 1. XRF, BET and TPD tests results of fresh catalyst.

XRF			BET		TPD	
Comp.	Starting gel	Final catalyst			Temperature range (C)	mmolt-Butylamin/gcat
Al	43.40 Wt%	48.63 Wt%	Surface area (m^2/gCat)	468	150-300	0.210
Si	6.78 Wt%	7.73 Wt%	Average particle size (mm)	1.6	350-450	0.224
P	49.82 Wt%	43.65 Wt%	Micropore volume (cm^3/gcat)	0.25	450-600	0.038

Table 2. Validation parameters.

Validation parameters	Correlation coefficient	RMSE
Value	0.9829	0.00702

Table 3. Model parameters of best fit.

Model Parameters	Value	Dimension
A	0.5543	gr Coke. gr Catalyst^{-1}. °C^{-1}
B	-0.16079	gr Coke. gr MeOH. hr^{-1}
C	0.07995	hr^{-1}
D	-6.6668	hr^{-1}
E	6.7794	Dimensionless
F	1.0873	Dimensionless
G	0.52872	Dimensionless
H	2.2983	Dimensionless